ANTIOXIDANTS & REDOX SIGNALING
Volume 26, Number 4, 2017

DOI: 10.1089/ars.2015.6548

Discoveries

FORUM ORIGINAL RESEARCH COMMUNICATION

GSNOR Deficiency Enhances *In Situ* Skeletal Muscle Strength, Fatigue Resistance, and RyR1 S-Nitrosylation Without Impacting Mitochondrial Content and Activity

Younghye Moon,[1] Yenong Cao,[1,2] Jingjing Zhu,[1] Yuanyuan Xu,[3] Wayne Balkan,[2,4] Emmanuel S. Buys,[5] Francisca Diaz,[6] W. Glenn Kerrick,[3] Joshua M. Hare,[1,2,4] and Justin M. Percival[1]

Abstract

Aim: Nitric oxide (NO) plays important, but incompletely defined roles in skeletal muscle. NO exerts its regulatory effects partly though S-nitrosylation, which is balanced by denitrosylation by enzymes such as S-nitrosoglutathione reductase (GSNOR), whose functions in skeletal muscle remain to be fully deciphered.
Results: GSNOR null ($GSNOR^{-/-}$) tibialis anterior (TA) muscles showed normal growth and were stronger and more fatigue resistant than controls *in situ*. However, $GSNOR^{-/-}$ lumbrical muscles showed normal contractility and Ca^{2+} handling *in vitro*, suggesting important differences in GSNOR function between muscles or between *in vitro* and *in situ* environments. $GSNOR^{-/-}$ TA muscles exhibited normal mitochondrial content, and capillary densities, but reduced type IIA fiber content. GSNOR inhibition did not impact mitochondrial respiratory complex I, III, or IV activities. These findings argue that enhanced $GSNOR^{-/-}$ TA contractility is not driven by changes in mitochondrial content or activity, fiber type, or blood vessel density. However, loss of GSNOR led to RyR1 hypernitrosylation, which is believed to increase muscle force output under physiological conditions. cGMP synthesis by soluble guanylate cyclase (sGC) was decreased in resting $GSNOR^{-/-}$ muscle and was more responsive to agonist (DETANO, BAY 41, and BAY 58) stimulation, suggesting that GSNOR modulates cGMP production in skeletal muscle.
Innovation: GSNOR may act as a ''brake'' on skeletal muscle contractile performance under physiological conditions by modulating nitrosylation/denitrosylation balance.
Conclusions: GSNOR may play important roles in skeletal muscle contractility, RyR1 S-nitrosylation, fiber type specification, and sGC activity. *Antioxid. Redox Signal*. 26, 165–181.

Keywords: nitric oxide, GSNOR, sGC, fatigue, S-nitrosylation, mitochondria

Introduction

NITRIC OXIDE (NO) plays many important roles in the skeletal muscle, where it is primarily synthesized by differentially localized nNOSμ and nNOSβ splice variants (38, 46, 49, 58). NO from neuronal nitric oxide synthase (nNOS) has been implicated in the regulation of skeletal muscle oxidative–glycolytic fiber type balance, growth, atrophy, strength, fatigue resistance, local blood delivery and glucose uptake during contraction, insulin sensitivity, mitochondrial biogenesis, and mitochondrial activity (19, 36, 44, 45, 48, 49, 56, 63, 64). The mechanisms by which NO performs these diverse functions in skeletal muscle are unclear.

Strict control of the site of NO synthesis represents an important mechanism facilitating NO signaling diversity. However, different NO signal propagation modes also represent an additional level of regulatory control that contributes to diversity. NO signals can be propagated through cGMP-dependent

[1]Department of Molecular and Cellular Pharmacology and [2]The Interdisciplinary Stem Cell Institute, University of Miami Miller School of Medicine, Miami, Florida.
Departments of [3]Physiology and Biophysics and [4]Medicine, University of Miami Miller School of Medicine, Miami, Florida.
[5]Department of Anesthesia, Critical Care and Pain Medicine, Anesthesia Center for Critical Care Research, Harvard Medical School, Massachusetts General Hospital Boston, Boston, Massachusetts.
[6]Department of Neurology, University of Miami Miller School of Medicine, Miami, Florida.

Innovation

Nitric oxide exerts its regulatory effects though S-nitrosylation, which is balanced by denitrosylation by enzymes such as S-nitrosoglutathione reductase (GSNOR). GSNOR function in skeletal muscle remains to be deciphered. Using GSNOR$^{-/-}$ mice, we provide evidence that GSNOR may regulate type IIA fiber type specification and soluble guanylate cyclase activity. Importantly, we also provide evidence that GSNOR may act as a ''brake'' on skeletal muscle contractility under physiological conditions, potentially through modulation of RyR1 S-nitrosylation. These data argue that GSNOR-modulated denitrosylation/nitrosylation balance is an important redox regulator of skeletal muscle contractile performance under physiological conditions.

pathways, where NO directly binds and activates soluble guanylate cyclase (sGC) to synthesize cyclic guanosine monophosphate (cGMP) (20, 28). Skeletal muscle cGMP-dependent NO signaling has emerged as an important drug target in dystrophinopathies (47). NO can also exert its regulatory effects on protein structure and function through S-nitrosylation of cysteine thiols (32, 34). The functions of NO in skeletal muscle that are mediated by cGMP-dependent signaling or by S-nitrosylation remain to be fully elucidated.

The importance of S-nitrosylation in skeletal muscle is highlighted by studies of the RyR1 Ca^{2+} release channel, an essential player in excitation–contraction coupling (33). Under physiological conditions, which include low O_2 concentrations, nNOSμ-mediated S-nitrosylation of cysteine 3536 of RyR1 increases open channel probability, leading to greater Ca^{2+} release and increased muscle force production (5, 23, 24, 59–61). The mechanisms modulating physiological RyR1 S-nitrosylation remain to be fully understood. In contrast, under pathological conditions, RyR1 hypernitrosylation can lead to ''Ca^{2+} leak'' (increased open channel probability), which contributes to skeletal muscle damage and weakness in many pathological states, including: Duchenne and Becker muscular dystrophies, β-sarcoglycanopathy, sarcopenia, malignant hyperthermia, and rheumatoid arthritis (4, 7, 8, 21, 31, 39, 67). These findings collectively suggest a somewhat paradoxical scenario where increased RyR1 S-nitrosylation could be either beneficial or detrimental to skeletal muscle depending on the cellular context. Thus, the physiological consequences of increased RyR1 S-nitrosylation and the roles of S-nitrosylation, more generally in skeletal muscle, remain to be determined.

The degree of S-nitrosylation is balanced by denitrosylation, which is regulated by enzymes such as S-nitrosoglutathione reductase (GSNOR), which acts as a denitrosylase. GSNOR degrades S-nitrosoglutathione (GSNO) and promotes glutathione (GSH) formation, thereby favoring a reduction in S-nitrosylation (26). Skeletal muscle contains a large pool of active GSNOR, the functions of which remain unclear (6a). However, consistent with a deleterious role for increased S-nitrosylation, GSNOR null mice may exhibit peripheral neuropathy and skeletal muscle dysfunction; whereas supraphysiological GSNO levels may promote weakness in skinned skeletal muscles *in vitro* (22, 43, 65). Thus, we hypothesize that loss of GSNOR will drive skeletal muscle weakness under physiological conditions.

To test our hypothesis and elucidate GSNOR function in skeletal muscle, we investigated muscle integrity and function in mice lacking GSNOR (GSNOR$^{-/-}$). GSNOR null tibialis anterior (TA) and lumbrical muscles displayed no evidence of atrophy or weakness. In fact, GSNOR$^{-/-}$ TA muscles were stronger and more fatigue resistant than controls and enhanced contractility was associated with RyR1 hypernitrosylation, providing a plausible mechanism. Differences in muscle response to GSNOR inhibition both *in situ* and *in vitro* were not unexpected and may reflect differences in GSNOR function between muscles or between *in vitro* and *in situ* environments. Increases in capillary density and oxidative fiber composition were ruled out as mechanisms underpinning enhanced contractility. GSNOR inhibition had no impact on mitochondrial content or respiratory chain complex I, III, and IV activities, providing evidence against a mitochondrial-based explanation for enhanced muscle contractility. Interestingly, control experiments designed to confirm that the effects of GSNOR inhibition were cGMP independent showed that sGC activity was attenuated in resting GSNOR$^{-/-}$ muscle. In addition, sGC in GSNOR$^{-/-}$ muscle was more responsive to distinct agonist classes, indicating a novel link between GSNOR and sGC and that GSNOR inhibition could impact cGMP signaling. Collectively, these data argue against the proposition that GSNOR inhibition or RyR1 hypernitrosylation alone is sufficient to drive skeletal muscle dysfunction. Importantly, these findings suggest roles for GSNOR denitrosylase in muscle contractility, fiber type specification, and mitochondrial respiratory chain function.

Results

GSNOR deficiency does not impair skeletal muscle hypertrophy or induce atrophy

nNOS expression and function varies between muscles (38, 49). Therefore, we investigated the possibility of muscle-specific differences in GSNOR expression. Normalized GSNOR protein expression was not significantly different between all skeletal muscle types investigated (Fig. 1A and Supplementary Fig. S1A; Supplementary Data are available online at www.liebertpub.com/ars). Next, we evaluated the impact of GSNOR deficiency on body and muscle mass. Six-month-old GSNOR$^{-/-}$ mice exhibited a significant 18% reduction in body mass, as previously reported (Fig. 1B and Supplementary Table S1) (14, 43). Accordingly, there was a reduction in glycolytic TA and oxidative soleus muscle masses (Fig. 1C, E). However, when TA and soleus muscles masses were normalized to body mass, no significant difference was observed (Fig. 1D, F and Supplementary Table S1). These results suggested that reductions in muscle mass occurred because GSNOR$^{-/-}$ mice were smaller. Supporting this possibility was the finding that nose-to-tail lengths of GSNOR$^{-/-}$ mice were significantly shorter than those of wild-type controls (WT: 9.74 ± 0.11 cm, GSNOR$^{-/-}$: 9.17 ± 0.1, $p < 0.01$).

To exclude atrophy as a causal factor in reduced muscle size, we measured the expression of two muscle-specific E3 ubiquitin ligases MuRF1 and Atrogin-1 whose expression is upregulated in atrophic muscles (9). Neither MuRF1 nor Atrogin 1 mRNA expression was significantly affected in GSNOR$^{-/-}$ muscle, arguing against the induction of muscle atrophy (Fig. 1G). These data were corroborated by findings that the cross-sectional areas and feret diameters of type IIB, IIX, and IIA myofibers of GSNOR$^{-/-}$ TA muscles were similar

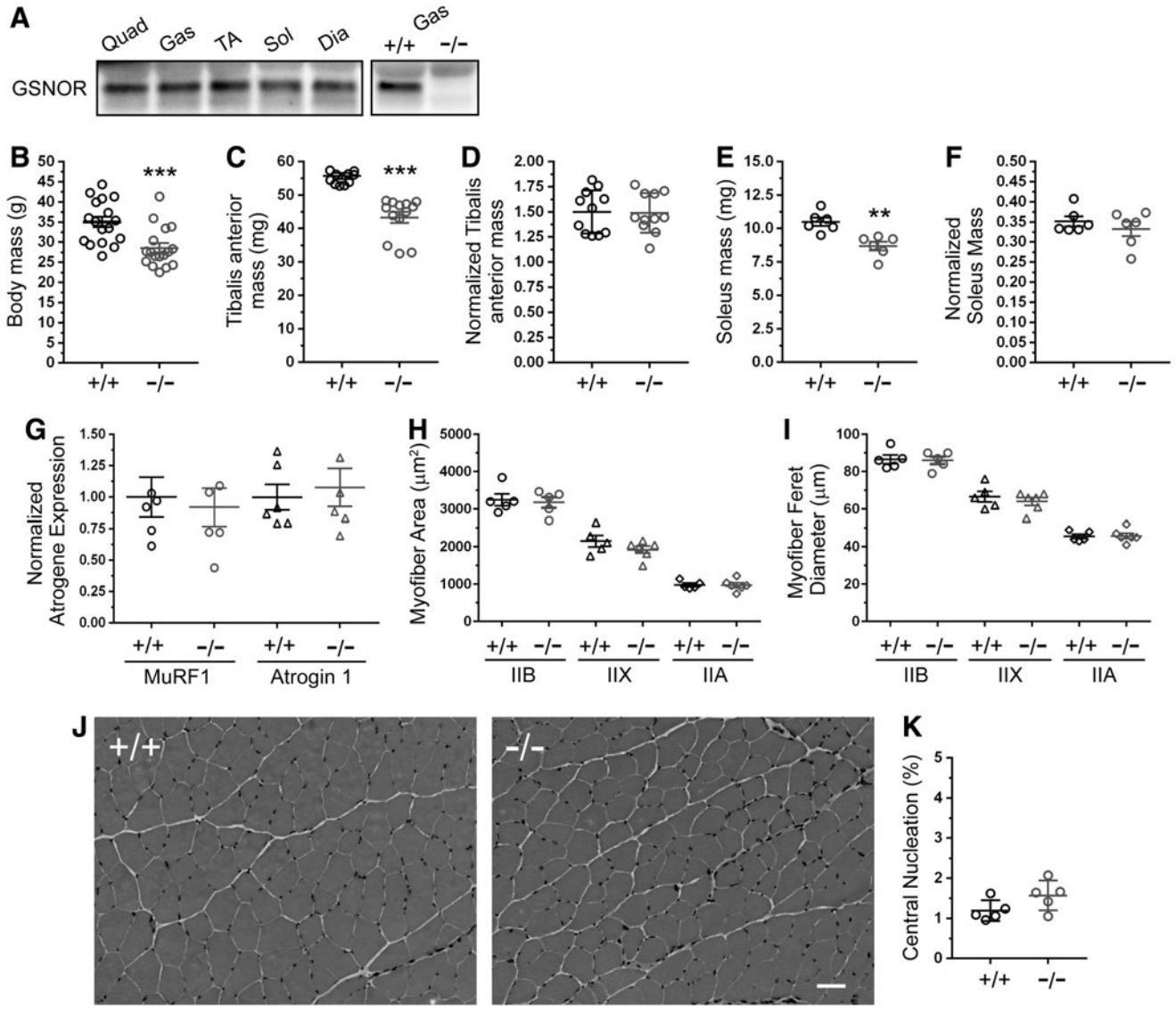

FIG. 1. GSNOR is dispensable for hypertrophic growth of skeletal muscle, and its absence does not induce atrophy. (A) Expression profile of GSNOR protein in oxidative and glycolytic skeletal muscles. Representative Western blots showing GSNOR protein expression in 3 month-old quad (quadriceps), gas (gastrocnemius), TA (tibialis anterior), sol (soleus), and dia (diaphragm) skeletal muscles. Representative Western blot confirming GSNOR antibody specificity using wild-type (WT, +/+) and GSNOR$^{-/-}$ (–/–) gastrocnemius muscle. $n = 3$. B-K represent data from 6 month-old mice. **(B)** Body masses of GSNOR$^{-/-}$ mice were significantly smaller than WT. $n = 17$. **(C)** TA masses were reduced in GSNOR$^{-/-}$ mice compared with WT controls. **(D)** TA masses normalized to body mass were similar between WT and GSNOR$^{-/-}$ mice. For **(C, D)**, $n = 11$ for WT and 13 for GSNOR$^{-/-}$ mice. **(E)** Soleus masses were decreased in GSNOR$^{-/-}$ mice compared with WT. **(F)** Soleus mass normalized to body mass did not differ between WT and GSNOR$^{-/-}$ mice. For **(E, F)**, $n = 6$ for each group. **(G)** Normalized expression of MuRF1 and Atrogin-1 mRNA (muscle-specific biomarkers of atrophy). MuRF1 and Atrogin 1 expression was affected by loss of GSNOR. $n = 6$ for all groups. **(H)** Cross-sectional area of type IIB, IIX, and IIA fibers in TA muscles from GSNOR$^{-/-}$ mice was unaffected, suggesting normal muscle hypertrophy. **(I)** Feret diameters of type IIB, IIX, and IIA fibers were also similar between WT and GSNOR$^{-/-}$ TA. For **(H, I)**, $n = 5$ for all groups. **(J)** Representative images of hematoxylin- and eosin-stained WT and GSNOR$^{-/-}$ TA muscles. GSNOR$^{-/-}$ muscles exhibited no overt signs of myopathy or dystrophy. $n = 10$ and 11 for WT type and GSNOR$^{-/-}$ mice, respectively. Scale bar: 50 μm. **(K)** The fraction of myofibers with centrally localized myonuclei, a biomarker of muscle cells that have undergone degeneration/regeneration. The fraction of centrally nucleated fibers was similar between WT and GSNOR$^{-/-}$ TA muscle, supporting normal muscle integrity. $n = 5$. Bars on graphs represent mean ± standard error of the mean. $^{**}p < 0.01$, $^{***}p < 0.001$. GSNOR, S-nitrosoglutathione reductase; WT, wild type

to controls (Fig. 1H, I). Total muscle cell number was also not significantly different between wild-type and GSNOR$^{-/-}$ muscles (data not shown). Histological analyses of GSNOR$^{-/-}$ muscle revealed no overt signs of myopathy or dystrophy, such as increased myofiber central nucleation, a biomarker of muscle degeneration/regeneration (Fig. 1J, K). Indeed, GSNOR$^{-/-}$ muscles were histologically indistinguishable from wild-type controls, supporting normal muscle integrity. Taken together, these data suggest that muscle growth and integrity is normal in the absence of active GSNOR.

GSNOR denitrosylase inhibits skeletal muscle strength and fatigue resistance in vivo

To gain the first insights into GSNOR function in skeletal muscle contractility under physiological conditions, we determined the isometric tetanic and twitch properties of TA muscles in anesthetized GSNOR$^{-/-}$ mice. There was no significant difference in maximal tetanic force output between GSNOR null and control TA muscles (Fig. 2A). Remarkably, GSNOR$^{-/-}$ muscles were significantly stronger than wild-type muscles, with greater specific force output (maximal tetanic force normalized to the muscle cross-sectional area) than wild-type controls (Fig. 2B). These data indicated that denitrosylation by GSNOR may negatively modulate muscle strength.

Skeletal muscle strength or force output is dependent on stimulation frequency. Therefore, we examined the impact of

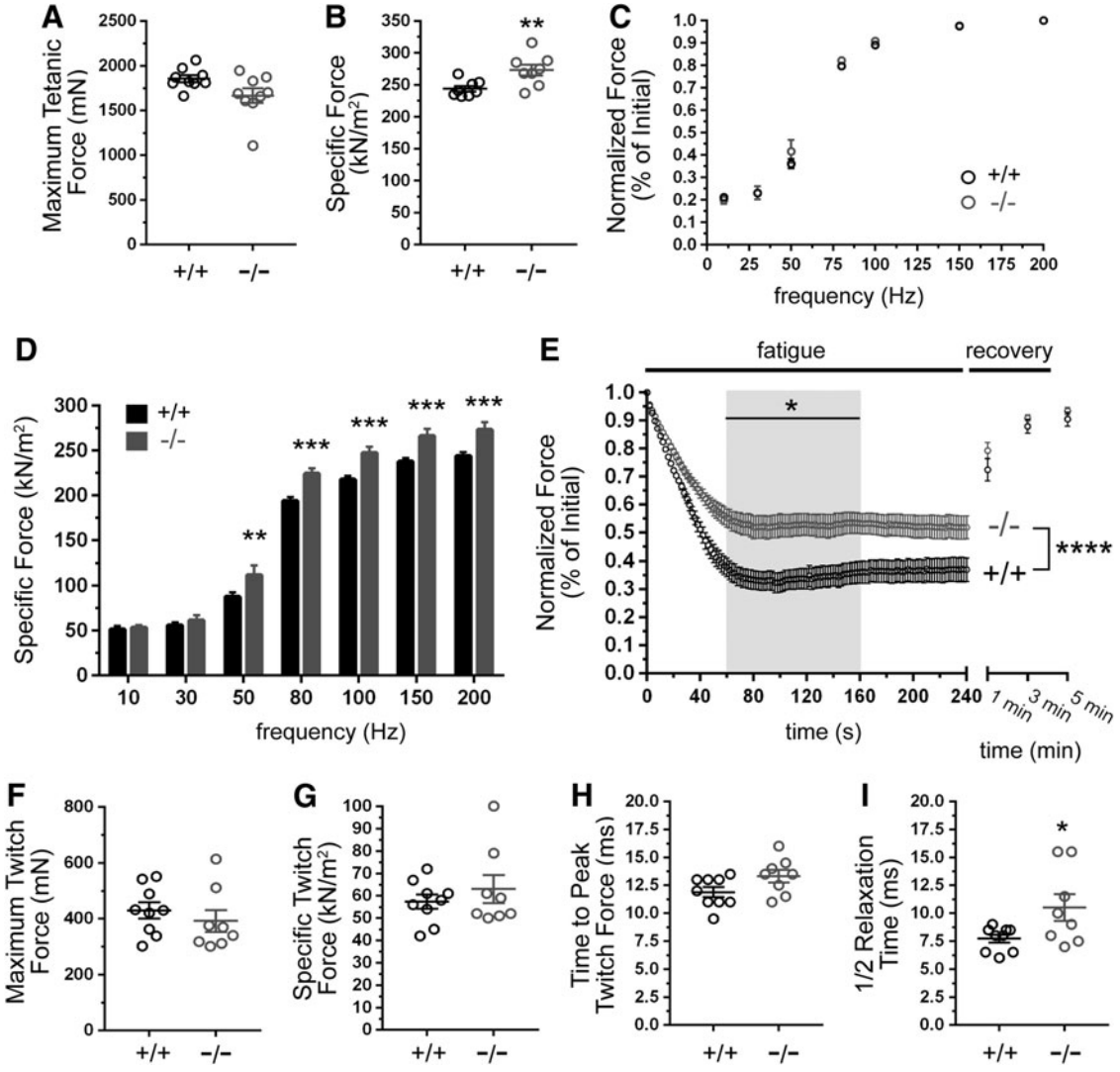

FIG. 2. Inhibition of GSNOR-mediated denitrosylation enhances skeletal muscle strength and fatigue resistance. **(A–D)** The isometric tetanic force-generating capacity of TA muscles in anesthetized 6 month-old wild-type (WT, +/+) and GSNOR$^{-/-}$ (−/−) mice. **(A)** Maximum tetanic force output was similar between GSNOR$^{-/-}$ and WT muscles. **(B)** Specific force was significantly increased in GSNOR$^{-/-}$ TA, indicating increased muscle strength. For **(A, B)**, $n=9$ for both groups. **(C)** Tetanic force output, normalized to initial force, was similar between WT and GSNOR$^{-/-}$ TA muscles at all stimulation frequencies, suggesting normal neuromuscular synapse function. $n=8$ for both groups. **(D)** Specific force was unaffected at stimulation frequencies <50 Hz in GSNOR$^{-/-}$ muscle; however, GSNOR$^{-/-}$ muscles were significantly stronger than WT controls at frequencies between 50 and 200 Hz. $n=8$ for both groups. **(E)** Fatigue resistance and post–fatigue force recovery of TA muscles. GSNOR$^{-/-}$ mice sustained significantly greater force output during the 60–160 s period (*gray box*), indicating enhanced fatigue resistance. Force recovery after 1, 3, and 5 min was similar between WT and GSNOR$^{-/-}$ mice. $n=9$ and 8 for wild-type and GSNOR$^{-/-}$ groups, respectively. **(F–I)** Impact of GSNOR deficiency on the isometric twitch properties of TA muscles *in vivo*. **(F)** Maximum isometric twitch force did not differ significantly between WT and GSNOR$^{-/-}$. $n=9$ and 8 for wild-type and GSNOR$^{-/-}$ groups, respectively. **(G)** Specific isometric twitch forces were not significantly different between GSNOR$^{-/-}$ and WT muscles. **(H)** The time taken to reach peak (maximum) twitch force in GSNOR$^{-/-}$ muscle was not different from WT. **(I)** The time taken to return to half-maximum twitch force was significantly ($p<0.05$) longer in GSNOR$^{-/-}$ muscle compared with WT, consistent with enhanced muscle fatigue resistance. *$p<0.05$, **$p<0.01$, and ***$p<0.001$.

GSNOR deficiency on force output at different stimulation frequencies. Normalized force output at frequencies between 10 and 200 Hz was indistinguishable between wild-type and GSNOR$^{-/-}$ muscle, consistent with normal gross neuromuscular and motor neuron function (Fig. 2C). Interestingly, although specific force was unaffected at stimulation frequencies less than 50 Hz, it was significantly increased between 50 and 200 Hz in GSNOR$^{-/-}$ muscle (Fig. 2D). Higher force output at lower stimulation frequencies may enhance fatigue resistance, since muscles can operate at a lower fraction of their maximum force generating capacity. Therefore, we tested whether loss of GSNOR augmented muscle fatigue resistance. Indeed, GSNOR$^{-/-}$ muscles exhibited a marked resistance to fatigue relative to wild-type controls (Fig. 2E). After an initial decline in force lasting $\sim$60 s, GSNOR$^{-/-}$ muscles sustained significantly higher normalized force output between 60 and 160 s relative to controls (Fig. 2E). Both control and GSNOR$^{-/-}$ muscles exhibited normal force recovery at 1, 3, and 5 min after the fatiguing period (Fig. 2E).

To further understand how GSNOR depletion enhanced skeletal muscle strength and fatigue resistance, we investigated TA muscle isometric twitch properties (Fig. 2F–I). Twitch properties are a function of fiber type and intracellular Ca^{2+} flux, both of which can modulate skeletal muscle force output. Maximum twitch force, specific twitch force, and time to peak (maximum) twitch force in GSNOR$^{-/-}$ muscles did not differ significantly from wild-type controls (Fig. 2F–H, respectively). However, twitch relaxation times were significantly longer in GSNOR$^{-/-}$ muscles (Fig. 2I). Slower relaxation times are typically found in more fatigue-resistant muscle types and may suggest changes in fiber type and/or slowed Ca^{2+} return to the sarcoplasmic reticulum. Collectively, these data support GSNOR-mediated denitrosylation as a regulatory mechanism that negatively modulates skeletal muscle exercise performance.

GSNOR deficiency leads to RyR1 hypernitrosylation

Next, we focused on investigating how GSNOR deficiency may enhance TA muscle contractility. Skeletal muscle force-generating capacity is determined, in part, by stimulatory NO or GSNO-mediated RyR1 S-nitrosylation at low physiological O_2 tensions (33). Note that this stimulatory activity is abrogated at high or normoxic O_2 tensions as seen in *in vitro* studies. Thus, increased RyR1 S-nitrosylation could contribute to increased GSNOR$^{-/-}$ TA skeletal muscle contractility under physiological conditions. To test RyR1 hypernitrosylation as a potential causal factor in the enhanced force output of GSNOR$^{-/-}$ TA skeletal muscle, RyR1 S-nitrosylation was measured by S-nitrosothiol resin-assisted capture (SNO-RAC) (25). Wild-type skeletal muscle exhibited low levels of S-nitrosylated RyR1 in the presence of ascorbate, as expected (Fig. 3A). In contrast, loss of GSNOR significantly increased RyR1 S-nitrosylation in both gastrocnemius (Fig. 3A, B) and TA muscles (Fig. 3C). RyR1 protein expression was unaffected in GSNOR$^{-/-}$ gastrocnemius (Fig. 3D)

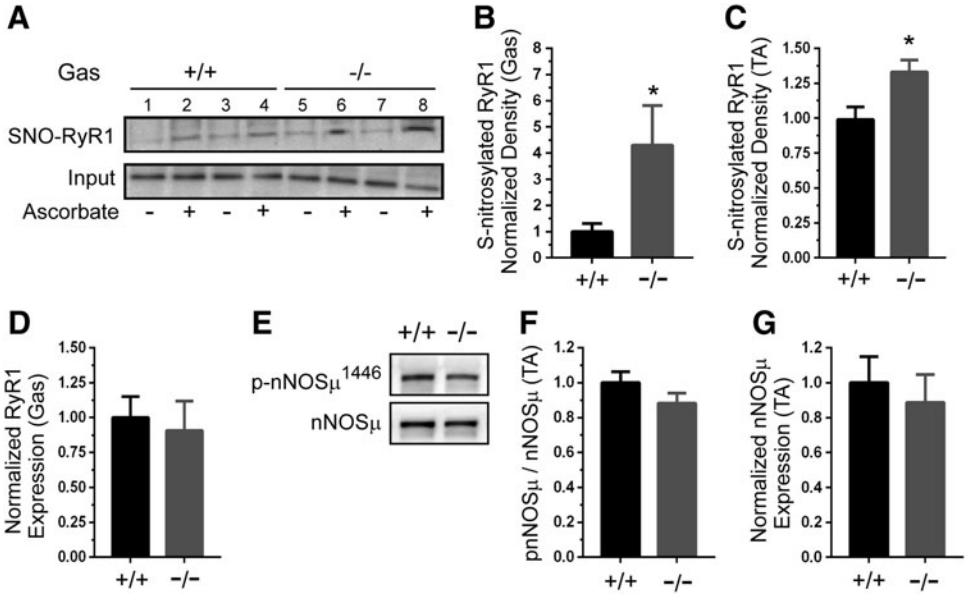

FIG. 3. GSNOR negatively regulates RyR1 Ca^{2+} channel S-nitrosylation. Determination of RyR1 S-nitrosylation status using SNO-RAC assay. Ascorbic acid, which converts nitrosothiol groups to thiols, was included as a specificity control. **(A)** RyR1 S-nitrosylation was increased in GSNOR$^{-/-}$ gastrocnemius. *Upper panel*: representative Western blot showing two wild-type (+/+) control (lanes 1–4) and two GSNOR$^{-/-}$ gastrocnemius samples (lanes 5–8). *Lower panel*: representative blot showing RyR1 input. **(B)** Quantitation revealed a marked approximately four-fold increase in RyR1 S-nitrosylation in the gastrocnemius (gas). **(C)** RyR1 hypernitrosylation also occurred in GSNOR$^{-/-}$ tibialis anterior muscles. **(D)** Gastrocnemius RyR1 protein expression was unaffected by loss of GSNOR. **(E)** Levels of nNOSμ and activated (Ser^{1446} phosphorylated) nNOSμ were determined. Representative Western blots showing expression of nNOSμ and active ser^{1446} phosphorylated nNOSμ in WT and GSNOR$^{-/-}$ TA muscle. **(F)** Quantitative analysis showed that the fraction of active ser^{1446} phosphorylated nNOSμ was unaffected by GSNOR depletion. **(G)** Quantitative analysis showed that nNOSμ protein expression was similar between WT and GSNOR$^{-/-}$ mice. A to D, $n=8$ and 7, for WT and GSNOR$^{-/-}$ groups, respectively. E to G, $n=6$ for all groups. * $p<0.05$. SNO-RAC, S-nitrosothiol resin-assisted capture.

and TA muscles (not shown). These data support GSNOR as an important negative regulator of RyR1 S-nitrosylation. Expression of the SERCA1 Ca^{2+} pump, another important player in excitation–contraction coupling, was similarly unaffected in $GSNOR^{-/-}$ muscle (Supplementary Fig. S2A).

Increases in RyR1-associated nNOSμ activity may also contribute to RyR1 hypernitrosylation (21, 39, 67). To test the possibility that nNOSμ was also driving RyR1 hypernitrosylation, we determined nNOSμ protein expression and the fraction of active serine^{1446} phosphorylated nNOSμ (35, 52). nNOSμ expression and the fraction of ser^{1446} phosphorylated nNOSμ were unaffected in $GSNOR^{-/-}$ muscles, suggesting that nNOSμ was not driving RyR1 hypernitrosylation (Fig. 3E–G and loading controls, Supplementary Fig. S1B). iNOS was undetectable in wild-type and $GSNOR^{-/-}$ skeletal muscles and, thus, unlikely to play a role in RyR1 hypernitrosylation (Supplementary Fig. S2B). Equivalent low levels of eNOS were found in both wild-type and $GSNOR^{-/-}$ muscle homogenates (Supplementary Fig. S2C). Activation of phosphorylation of eNOS at serine 1177 was also undetectable in resting muscles (Supplementary Fig. S2D). These findings argue against increased nNOSμ, iNOS, and eNOS expression or activity in driving RyR1 hypernitrosylation in GSNOR null mice. Taken together, these data suggest that RyR1 hypernitrosylation in $GSNOR^{-/-}$ muscle was primarily due to increased GSNO.

GSNOR null lumbrical muscles exhibit normal force output and Ca^{2+} handling in vitro

Enhanced contractility, RyR1 hypernitrosylation, and longer twitch relaxation times in $GSNOR^{-/-}$ null muscle suggested a possible change in Ca^{2+} handling. So, we simultaneously measured changes in force and intracellular Ca^{2+} $[Ca^{2+}]_i$ in intact paw lumbrical muscles *in vitro* to investigate increased Ca^{2+} flux as a contributing factor to the enhanced contractile performance of $GSNOR^{-/-}$ null muscle (66). Note that comparable methodologies for discerning changes in force and Ca^{2+} flux in TA muscles *in situ* remain to be developed. Representative data traces are shown in Supplementary Fig. S3. Unlike the TA, specific force was unaffected in $GSNOR^{-/-}$ lumbrical muscle (Fig. 4A). Both normalized $[Ca^{2+}]_i$ and force output were also unaffected at all stimulation frequencies (Fig. 4B). To recapitulate fatiguing conditions, lumbrical muscles were subject to 100 maximal tetanic stimulations separated by 0.5–8 s intervals. Stimulus intervals from 0.5 to 5 s significantly decreased force output in wild-type controls and $GSNOR^{-/-}$ muscle to a similar degree, indicating that lumbrical muscle fatigue resistance was unaffected by GSNOR loss (Fig. 4C). Also, unlike force output, $[Ca^{2+}]_i$ was similar between wild-type and $GSNOR^{-/-}$ muscles under progressively more fatiguing conditions (Fig. 4C). Therefore, in contrast to findings in the TA, these data suggest that GSNOR does not, or cannot, regulate force output and Ca^{2+} handling in lumbrical muscles *in vitro*. These data may reflect differences between *in vitro* and *in situ* environments of lumbrical and TA muscles, where the *in vitro* environment fails to fully mimic the *in situ* environment. Alternatively, they may reflect muscle-specific differences in GSNOR function.

$GSNOR^{-/-}$ muscles have decreased type IIA fiber content, but normal capillary density

Skeletal muscle fatigue resistance is a function of not only Ca^{2+} release but also other interdependent factors such as: oxidative fiber composition, mitochondrial content and activity, and blood vessel densities (2). Therefore, we investigated these factors as possible mechanisms to explain the enhanced fatigue resistance of $GSNOR^{-/-}$ muscle. To discern whether GSNOR depletion increased oxidative fiber content, which could increase fatigue resistance, we determined the frequency of type IIX, IIB, IIA, mixed I/IIA, and type I myosin-positive fibers in TA muscles. Type IIX and IIB, as

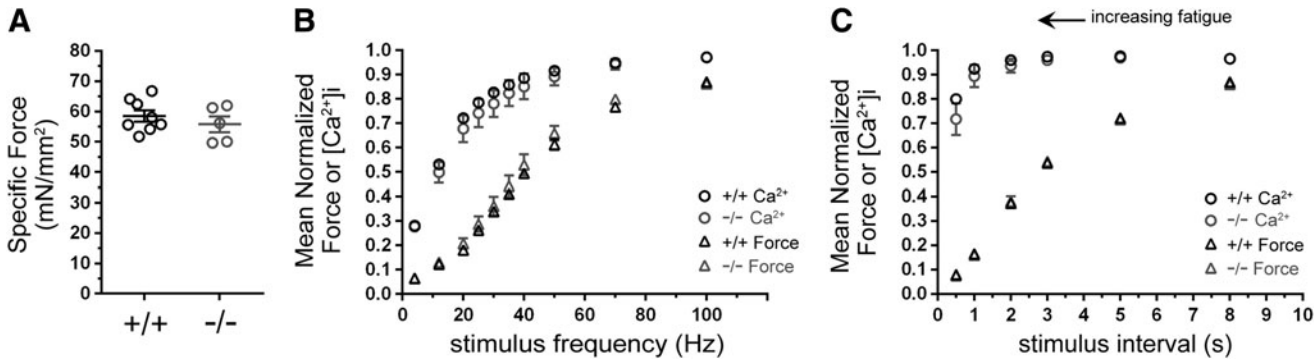

FIG. 4. GSNOR denitrosylase is dispensable for normal Ca^{2+} handling, strength, and fatigue resistance in lumbrical skeletal muscles *in vitro*. Force output and intracellular Ca^{2+} levels were simultaneously measured in intact wild-type (WT, +/+) and $GSNOR^{-/-}$ (–/–) lumbrical muscles *in vitro*. $n = 7$ and 5 for WT and $GSNOR^{-/-}$ groups. **(A)** Specific force was not affected by the loss of GSNOR. **(B)** Mean normalized tetanic force output was unaffected by GSNOR deficiency at submaximal and maximal (100 Hz) stimulation frequencies. Similarly, mean normalized intracellular Ca^{2+} $[Ca^{2+}]_i$ concentrations in $GSNOR^{-/-}$ muscle were similar to WT controls at all stimulation frequencies. **(C)** The impact of muscle fatigue on force output and Ca^{2+} transients in WT and $GSNOR^{-/-}$ lumbrical muscle. To induce muscle fatigue, WT and $GSNOR^{-/-}$ lumbrical muscles were subjected to stimulation at progressively shorter intervals (0.5 to 8 s) between stimuli. As expected, mean normalized force output in WT muscle decreased proportionately with a shorter stimulus interval, indicating greater muscle fatigue. Unlike force, $[Ca^{2+}]_i$ did not decrease significantly. Loss of GSNOR had no impact on force output or $[Ca^{2+}]_i$ compared with WT at all stimulus intervals.

well as type I/IIA and I fiber types, were unaffected in GSNOR$^{-/-}$ muscle (Fig. 5A). Interestingly, type IIA fiber incidence was 41% lower in muscles from GSNOR$^{-/-}$ mice than from wild-type mice. However, reduced numbers of type IIA fibers would favor decreased fatigue resistance, and, therefore, cannot explain enhanced fatigue resistance.

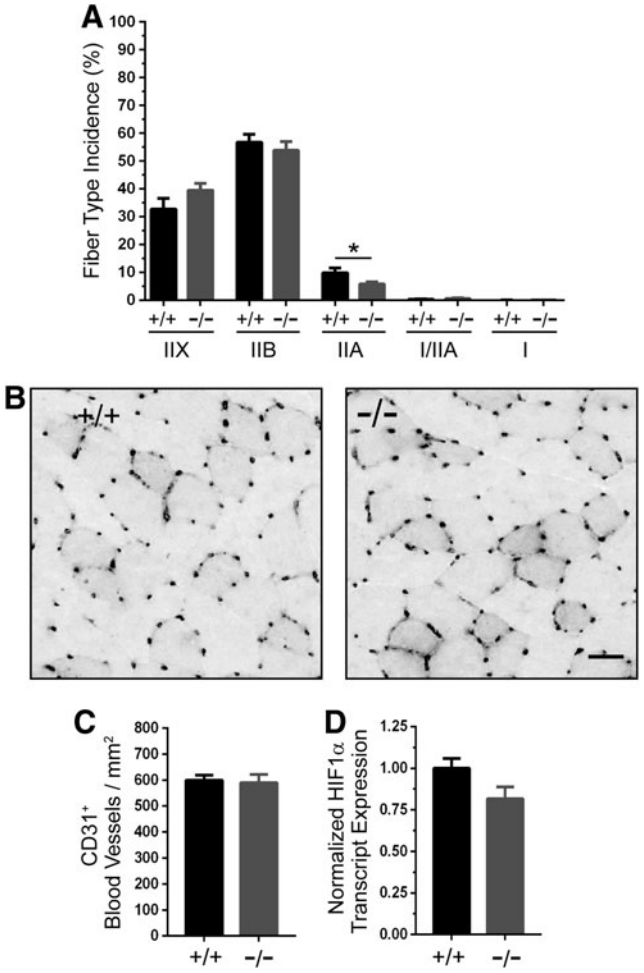

FIG. 5. Enhanced muscle fatigue resistance in GSNOR null mice is not driven by increased oxidative fiber type or blood vessel density. **(A)** Quantitation of fiber type incidence (percent of total fiber number) in GSNOR$^{-/-}$ tibialis anterior muscle. GSNOR deficiency had no impact on type IIX, IIB, I/IIA, and type I incidence, but it significantly decreased type IIA fiber content by 41%. Note that type I and type I/IIX make up only a few percent of fibers in the TA and were excluded from quantitation. $n=5$ and 6, for WT and GSNOR$^{-/-}$ groups, respectively. **(B)** To test whether enhanced fatigue resistance in GSNOR$^{-/-}$ muscle resulted from increased vascularization, we determined CD31 positive blood vessel density in TA muscle cryosections. Representative WT and GSNOR$^{-/-}$ images are shown, with CD31 labeling large blood vessels and capillaries that were more heavily concentrated around type IIX and IIA fibers. **(C)** Quantitation of CD31-positive blood vessels per mm^2 in TA muscles. CD31-positive blood vessel density did not differ between WT and GSNOR$^{-/-}$ TA muscles. $n=9$ and 6 for WT and GSNOR$^{-/-}$ groups, respectively. Scale bar: 30 μm. **(D)** HIF1α transcript expression was similar between WT and GSNOR$^{-/-}$ muscles. $n=6$ for both groups. *$p<0.05$.

Enhanced fatigue resistance could be attributable to increased capillary density in GSNOR$^{-/-}$ skeletal muscle, which would facilitate oxygen delivery and extraction during contraction. Indeed, GSNOR negatively regulates vasculogenesis in cardiac muscle *via* an HIF1α-dependent mechanism (40). Therefore, we measured the density of CD31-positive capillaries and blood vessels in TA skeletal muscles. As expected, capillaries were clustered at higher densities around the more oxidative fiber types; however, no qualitative difference between wild-type and GSNOR$^{-/-}$ muscle was observed (Fig. 5B). Quantitative image analysis showed that blood vessel

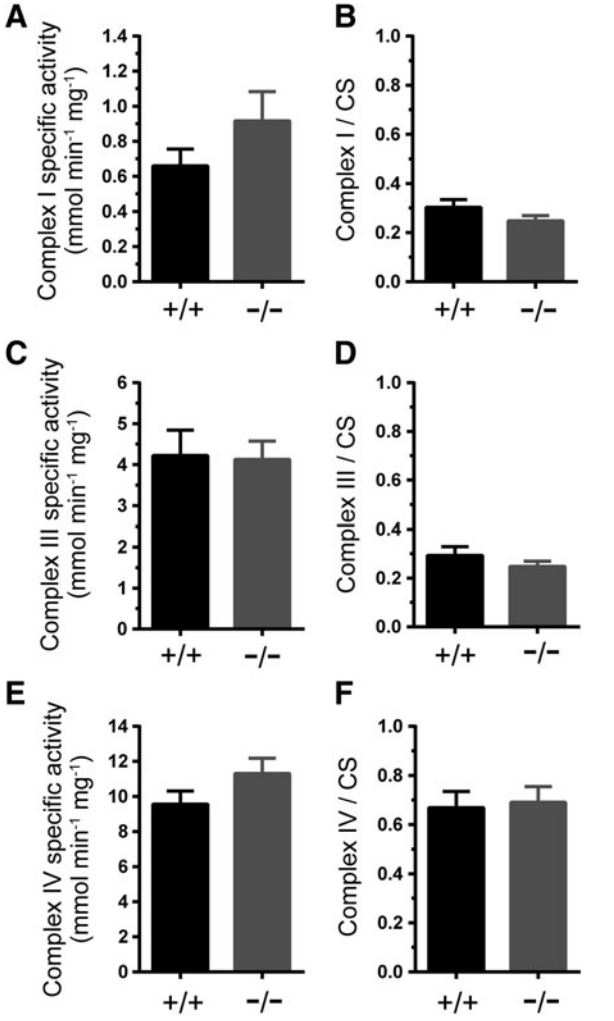

FIG. 6. Mitochondrial respiratory complex activity in GSNOR$^{-/-}$ muscle. To test whether increased mitochondrial activity could contribute to the enhanced contractility of GSNOR$^{-/-}$ tibialis anterior (TA) muscle, the specific activities and citrate synthase (activity)-normalized activities of mitochondrial respiratory chain complexes I, III, and IV were measured in wild-type (+/+) and GSNOR$^{-/-}$ TA muscles. **(A)** Complex I-specific activity. **(B)** Citrate synthase activity (CS)-normalized complex I-specific activity. **(C)** Complex III-specific activity. **(D)** CS activity-normalized complex III-specific activity. **(E)** Complex IV-specific activity. **(F)** CS activity-normalized complex IV-specific activity. $n=6$ for wild-type and GSNOR$^{-/-}$ groups, respectively. $n=6$ for all groups.

density was comparable between wild-type and GSNOR$^{-/-}$ muscle (Fig. 5C). HIF1α transcript expression was unaffected by the loss of GSNOR, which was consistent with normal vasculogenesis in GSNOR$^{-/-}$ muscle (Fig. 5D). Note that HIF1α protein expression was undetectable in both wild-type and GSNOR$^{-/-}$ muscle (not shown). These findings suggest that GSNOR does not regulate vasculogenesis in skeletal muscle, and that increased blood vessel density does not contribute to the enhanced contractility of GSNOR$^{-/-}$ muscle *in situ*. Collectively, these data strongly suggest that increased oxidative fiber type and blood vessel density do not contribute to enhanced fatigue resistance of GSNOR$^{-/-}$ muscles.

Loss of GSNOR does not impact skeletal muscle mitochondrial content or activity

Mitochondria play a crucial and firmly established role in meeting the energy demands of skeletal muscles and are an important target of NO (18, 27). Therefore, we tested whether enhanced GSNOR$^{-/-}$ TA contractility could result from increased mitochondrial function by determining the maximal catalytic (specific) activities of respiratory complexes I, III, and IV that can be modulated by NO (11, 16, 27). Loss of GSNOR did not impact the specific activities of complex I, III, or IV (Fig. 6A, C, E, respectively). Similarly, citrate synthase-normalized complex I, III, and IV activities were not significantly different between wild-type and GSNOR$^{-/-}$ TA muscle (Fig. 6B, D, F, respectively). Together, these findings suggest that GSNO may not regulate respiratory complex activity and argue against increased mitochondrial activity as a causal mechanism to explain enhanced TA muscle strength and fatigue resistance.

In addition to regulating respiration, NO may promote mitochondrial biogenesis in skeletal muscle cells and other cell types under some conditions (44, 45, 51). Therefore, we tested whether loss of GSNOR could increase mitochondrial content. Expression of the outer mitochondrial membrane protein VDAC1 was similar between wild-type and GSNOR$^{-/-}$ TA muscles (Fig. 7A, loading controls in Supplementary Fig. S1C). Although complex II subunit SDHB expression was higher in GSNOR$^{-/-}$ muscle, possibly reflecting a change in subunit stoichiometry, expression of subunits from complexes I, III, IV, and V was unaffected, arguing against increased mitochondrial biogenesis in GSNOR$^{-/-}$ muscle. (Fig. 7B, loading controls in Supplementary Fig. S1D). Similar results were seen in gastrocnemius muscle (Supplementary Fig. S4A–D). In addition, citrate synthase activity, a measure of mitochondrial content, was also unaffected by loss of GSNOR (Fig. 7C). Furthermore, the ratio of mitochondrial DNA to nuclear DNA was similar between control and GSNOR$^{-/-}$ TA muscle (Fig. 7D). In agreement, expression of PGC1α, a transcriptional coactivator activated by NO that promotes mitochondrial biogenesis, was comparable between wild-type and GSNOR$^{-/-}$ TA muscles (Fig. 7E). These data provide compelling evidence that loss of GSNOR does not drive mitochondrial biogenesis, arguing against biogenesis as a potential mechanism to explain the enhanced contractility of GSNOR$^{-/-}$ TA muscle.

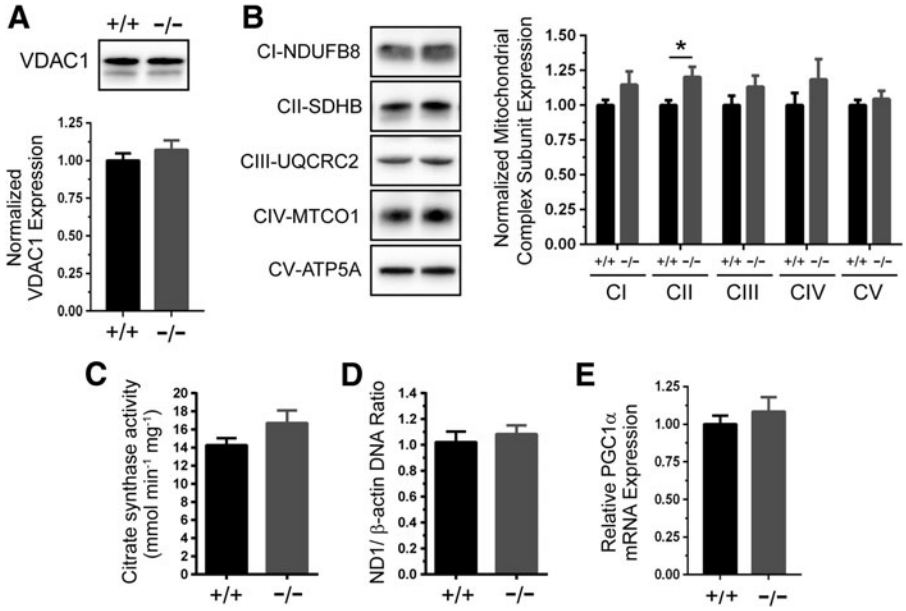

FIG. 7. GSNOR-deficient skeletal muscles have normal mitochondrial content. Mitochondrial biogenesis was investigated as a potential mechanism that could contribute to enhanced GSNOR$^{-/-}$ tibialis anterior (TA) muscle contractility. **(A)** Representative Western blot and densitometric quantitation of mitochondrial outer membrane VDAC1 protein expression in wild-type (+/+) and GSNOR$^{-/-}$ TA muscles. **(B)** Representative Western blots and densitometric quantitation of expression of subunits of mitochondrial respiratory chain complexes I through V in wild-type and GSNOR$^{-/-}$ TA muscles. Although complex II subunit SDHB expression was significantly higher in GSNOR$^{-/-}$ TA muscle, expression of subunits from all other complexes was unaffected, arguing against biogenesis. $^*p < 0.05$. **(C)** Citrate synthase activity, a biomarker of mitochondrial content, was similar between wild-type and GSNOR$^{-/-}$ TA muscle. **(D)** The ratio of ND1/β-actin DNA was unaffected by GSNOR deficiency. **(E)** mRNA expression of PGC1α, an important transcriptional regulator of mitochondrial biogenesis, was similar between WT and GSNOR$^{-/-}$ muscle. $n = 6$ for all groups.

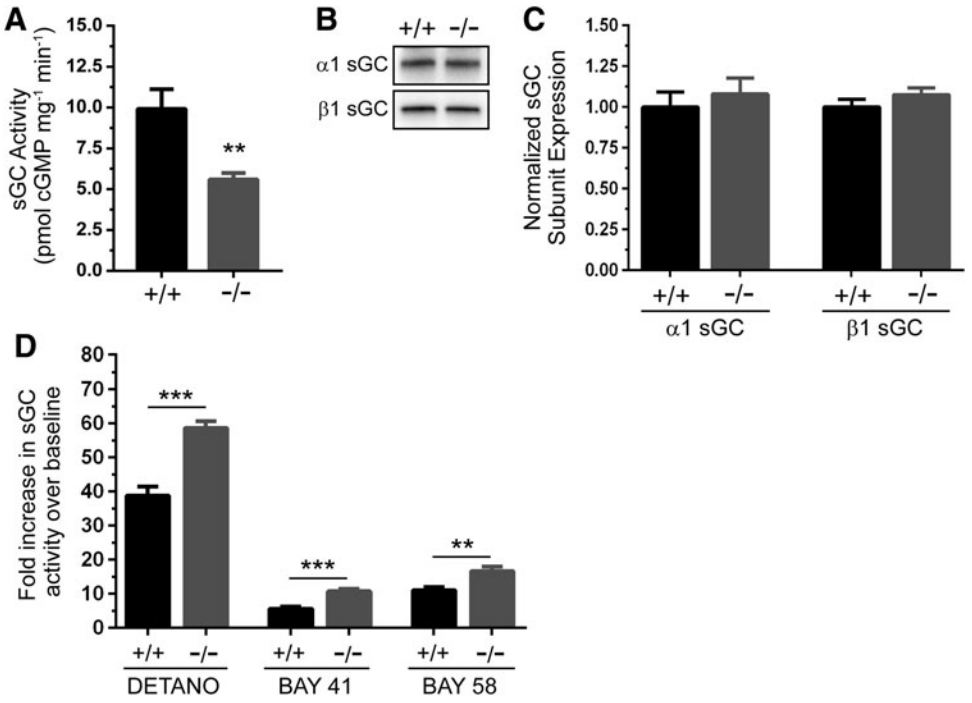

FIG. 8. GSNOR modulates cGMP synthesis by soluble guanylate cyclase. To test whether loss of GSNOR could impact cGMP-dependent NO signal transduction, soluble guanylate cyclase (sGC) expression and activity was measured in gastrocnemius muscles. **(A)** Baseline sGC activity was significantly reduced by 44% in GSNOR$^{-/-}$ muscle compared with wild-type controls. **(B)** Representative Western blot showing that $\alpha 1$ and $\beta 1$ sGC subunit expression was unaffected in GSNOR$^{-/-}$ muscle. **(C)** Densitometric quantitation confirmed that $\alpha 1$ and $\beta 1$ sGC subunit expression was unaffected by loss of GSNOR; therefore, reductions in activity were not due to reduced $\alpha 1\beta 1$ sGC expression. For **(A, B)**, $n = 6$ and 5 for WT and GSNOR$^{-/-}$ groups, respectively. **(D)** Fold increase sGC activity relative to baseline in response to NO donor DETANO, sGC stimulator BAY 41-2272 (BAY 41), or sGC activator BAY 58-2667 (BAY 58) in gastrocnemius muscle homogenates. DETANO, BAY 41, and BAY 58 increased sGC-mediated cGMP synthesis to a significantly greater degree in GSNOR$^{-/-}$ muscles than WT, suggesting enhanced responsiveness of sGC. For **(C, D)**, $n = 6$ for both groups. $^{**}p < 0.01$, $^{***}p < 0.001$.

GSNOR modulates cGMP synthesis by sGC

As an important control to provide evidence that the impact of GSNOR depletion on skeletal muscle was independent of effects on cGMP-based signaling pathways, we investigated sGC activity in GSNOR$^{-/-}$ muscles. If the positive impact of GSNOR depletion on muscle contractility *in situ* was cGMP independent, then we would expect no change in cGMP synthesis by sGC. GSNOR depletion significantly decreased sGC activity by 44% in resting skeletal muscle (Fig. 8A). $\alpha 1$ and $\beta 1$ sGC subunit expression was unaffected in GSNOR$^{-/-}$ muscle, suggesting that reduced sGC activity was not due to decreased sGC protein expression (Fig. 8B, C, loading controls in Supplementary Fig. S1E). Surprisingly, sGC activity in GSNOR$^{-/-}$ skeletal muscle was more responsive than wild type to agonists, including the NO donor DETANO, the sGC stimulator BAY 41-2272, and the sGC activator BAY 58-2667 (Fig. 8D). Indeed, the increase in sGC activity in GSNOR$^{-/-}$ muscle was 50% greater with DETANO and BAY 58-2667, and 90% greater with BAY 41-2272. Increased sGC S-nitrsylation was not apparent by SNO-RAC analysis (not shown). Nonetheless, these data suggest that GSNOR is necessary for normal sGC activity in resting skeletal muscle and that GSNOR-mediated denitrosylation modulates the responsiveness of cGMP synthesis by sGC. These data suggest that some phenotypes of GSNOR$^{-/-}$ muscles may be partly due to altered cGMP signaling.

Discussion

A key finding of the present study is that GSNOR, and denitrosylation more generally, may play an important role in modulating skeletal muscle force output under physiological conditions. Innervated and vascularized GSNOR$^{-/-}$ TA muscles were 12–27% stronger at maximal (200 Hz) and physiological submaximal (150 to 50 Hz) stimulation frequencies. This increase in strength is highly physiologically relevant considering that a difference of 22% represents the margin between dystrophic and wild-type muscle (50). GSNOR$^{-/-}$ TA muscles were also more fatigue resistant, with a 17% increase in force output between 60 and 160 s compared with controls and longer twitch relaxation times that are stereotypical of higher fatigue resistance. These data suggest that NO can modulate muscle fatigue resistance through an S-nitrosylation-/denitrosylation-dependent mechanism and that GSNOR acts as a brake on skeletal muscle force generation under physiological conditions.

These data also support and extend previous studies, indicating an important role for NO synthesized by nNOS in skeletal muscle fatigue (1, 19, 46, 48, 49). Using a similar approach, nNOS deficiency (primarily the loss of nNOSβ) substantially decreased both TA muscle fatigue resistance and postexercise force recovery (49). The findings in the present study support the possibility that NO regulates muscle fatigue resistance through S-nitrosylation-/denitrosylation-based mechanisms

under physiological conditions. Interestingly, force recovery after fatigue was normal in GSNOR$^{-/-}$ muscle, suggesting that GSNOR, and S-nitrosylation/denitrosylation more generally, does not play a role in postexercise force recovery.

The question then arises as to how GSNOR may modulate force production. Skeletal muscle force production can be enhanced by several factors such as increases in oxidative fiber content, mitochondrial content or activity, vascular density, and S-nitrosylation of the RyR1 Ca^{2+} channel. We found that type IIX and IIB fiber (glycolytic) content was unaffected in GSNOR$^{-/-}$ mice. However, oxidative type IIA fiber content was decreased, which was unexpected since greater fatigue resistance is often accompanied by increased type IIA content. The significance of the reduction in type IIA fibers remains unclear, but it may relate to metabolic changes in GSNOR$^{-/-}$ muscles. nNOS can regulate fiber composition, with nNOSμ suppressing type IIX fiber content (15, 49). Given that type IIX fiber composition was unchanged in GSNOR$^{-/-}$ mice, it is likely that IIX content is modulated through a cGMP-dependent nNOSμ signaling mechanism. However, these data do not support a role for altered fiber type specification as an important factor in the enhanced contractility of GSNOR$^{-/-}$ muscle.

Enhanced GSNOR$^{-/-}$ TA muscle contractility also did not appear to be driven by increased mitochondrial content or respiratory chain complex activity. Expression of mitochondrial proteins, including VDAC1 and specific subunits of respiratory complexes I through V, was unaffected by GSNOR deficiency. In addition, citrate synthase activity, mitochondrial DNA/nuclear DNA ratio, and PGC1α mRNA expression were not significantly different from controls, providing strong evidence for normal mitochondrial content in GSNOR$^{-/-}$ muscle. Although complex I activity can be regulated by NO and S-nitrosylation in other cell types, it was unaffected in GSNOR$^{-/-}$ TA muscle, consistent with a previous report that complex I activity in TA muscle was unaffected by loss of nNOSμ (17, 19, 30, 57). Similarly, complex IV activity, which is reversibly inhibited by NO, was also unaffected in GSNOR$^{-/-}$ TA muscles. Also, GSNO can inhibit complex III activity in cardiac sub-mitochondrial particles, whereas GSNOR depletion did not impact complex III activity in skeletal muscle, supporting differences in GSNOR function between heart and skeletal muscles (37, 40). Taken together, these data argue against increased mitochondrial respiratory chain activity as a mechanism to explain increased strength and fatigue resistance of GSNOR$^{-/-}$ TA muscles.

Increased capillary density was also ruled out as contributing to enhanced TA muscle contractility. Increases in capillary density in the vascular beds of skeletal muscle augment O_2 delivery and extraction, promoting fatigue resistance. Indeed, GSNOR deficiency can increase capillary density in cardiac muscle through mechanisms involving VEGF and S-nitrosylation of HIF1α (40). However, we found that capillary density was unaffected in GSNOR$^{-/-}$ TA muscles and that HIF1α transcript was unaffected, whereas HIF1α protein was undetectable (data not shown). These findings agree with a recent study suggesting that the primary source of skeletal muscle NO, nNOSμ, is dispensable for capillary density (6). These data suggest that angiogenesis is differentially regulated by GSNOR during skeletal and cardiac muscle development, and they argue against increased capillary density as an important factor in the augmented fatigue resistance of GSNOR$^{-/-}$ mice.

GSNOR depletion led to RyR1 hypernitrosylation in TA muscles. Given compelling evidence that S-nitrosylation of RyR1 positively regulates Ca^{2+} release and force development under physiological oxygen tensions and that RyR1 S-nitrosylation is increased in GSNOR$^{-/-}$ muscle (Fig. 3A–C), it is plausible that RyR1 hypernitrosylation could be a key contributing factor to the enhanced force output in GSNOR$^{-/-}$ TA muscle (5, 23, 24, 33, 59–62). Thus, our data suggest RyR1 hypernitrosylation as the best mechanism to explain the enhanced contractility of GSNOR$^{-/-}$ TA muscle, and to explain how GSNOR may act as a brake on skeletal muscle force generation under physiological conditions. It is important to note that we cannot show cause and effect, only association, between RyR1 hypernitrosylation and enhanced contractility of TA muscles. In addition, the involvement of other S-nitrosylated proteins cannot be ruled out as contributing factors. So, our interpretation of current evidence is that GSNOR-mediated denitrosylation may serve as a mechanism to modulate skeletal muscle exercise capacity by facilitating removal of NO functional groups from the RyR1 receptor.

Under pathological conditions, RyR1 hypernitrosylation is typically associated with skeletal muscle wasting and weakness and may be a secondary pathogenic feature of diverse pathological states, including: malignant hyperthermia, over-training, sarcopenia, rheumatoid arthritis, dystrophinopathy, and β-sarcoglycanopathy (3, 4, 7, 8, 21, 31, 39, 67). In these states, RyR1-mediated Ca^{2+} leak from the sarcoplasmic reticulum may aberrantly activate RyR1-associated nNOSμ, disrupting the tight temporal control of NO production and driving nitrosative stress and further pathogenic RyR1 hypernitrosylation (21, 31, 39, 67). In turn, pathogenic RyR1 hypernitrosylation induces further Ca^{2+} leak, leading to progressively more severe muscle damage and weakness. However, our data suggest that GSNOR inhibition, with concomitant RyR1 hypernitrosylation, can have a positive impact on muscle contractile performance. Collectively, these data suggest a fundamental difference between the impact of RyR1 hypernitrosylation resulting from inhibition of denitrosylation and that from Ca^{2+} leak-driven nitrosative stress. Since different sets of RyR1 cysteines may be modified by GSNO and nNOSμ under normal and pathological conditions, distinct RyR1 cysteine modification patterns may differentially impact muscle integrity and contractility in normal and diseased states (61). Therefore, RyR1 hypernitrosylation resulting from inhibition of denitrosylation may be beneficial to skeletal muscle, whereas hypernitrosylation resulting from nNOSμ-mediated nitrosative stress is deleterious. The differences between the causes and consequences of RyR1 hypernitrosylation under physiological and pathophysiological conditions represent an important area for further investigation.

However, in contrast to GSNOR$^{-/-}$ TA muscle, loss of GSNOR in intact lumbrical muscle did not impact Ca^{2+} handling, strength, fatigue resistance or rates of muscle relaxation, and activation *in vitro* (Fig. 4 and Supplementary Fig. S2). It is important to note that methods with comparable sensitivity for simultaneously measuring changes in force and Ca^{2+} in the TA or other intact muscles remain to be developed, so it is not possible to determine whether RyR1 Ca^{2+} channel hypernitrosylation impacted Ca^{2+} flux. At

present, it is unclear why GSNOR deficiency had different effects in TA and lumbrical muscles, so we can only speculate at present about possible explanations. One explanation is that GSNOR has muscle-specific functions where it modulates contractility in the TA, but not the lumbrical muscles. This would suggest muscle-specific differences in the role of denitrosylation, consistent with muscle-specific differences in nNOS expression, activity, and function (38, 49). In agreement, RyR1 S-nitrosylation was higher in gastrocnemius than in TA muscles. A second possibility is that there is a critical difference in the environment of the lumbrical and TA muscle that may abrogate the ability of GSNOR inhibition to impact contractility. Specifically, supraphysiological O_2 tensions found in the *in vitro* bath environment may prevent stimulatory RyR1 S-nitrosylation, which is believed to occur only under low O_2 tensions (23, 24, 60–62). We were unable to test this possibility due to the technical difficulty of using SNO-RAC on tiny lumbrical paw muscles. A third possibility is that GSNOR in a tissue outside of skeletal muscle may indirectly modulate muscle contractility and this mechanism of contractile control would be missing from *in vitro* studies. For example, muscle fatigue resistance is also a function of blood-mediated O_2 delivery and extraction, which is closely matched to the O_2 demands of contracting muscle (2). So, it is conceivable that improved cardiac output in GSNOR$^{-/-}$ mice could increase blood delivery to active muscles, promoting fatigue resistance. The mechanisms by which GSNOR inhibition promotes skeletal muscle strength and fatigue resistance represent an important future research direction.

More importantly, our findings in both GSNOR$^{-/-}$ lumbrical and TA muscles challenge previous propositions that inhibiting GSNOR or increasing GSNO or RyR1 S-nitrosylation causes skeletal muscle wasting *in vivo* and weakness in skinned skeletal muscles *in vitro* (22, 43). However, the physiological relevance of the *in vitro* effects of GSNO was questioned due to use of supraphysiological GSNO doses (65). GSNOR$^{-/-}$ mice were reported to exhibit neuromuscular dysfunction characterized by peripheral nerve dysfunction and damage, heightened pain sensitivity, muscle atrophy, and a reduction in grip strength (an indirect and unreliable measure of muscle strength) that were interpreted as evidence of myopathy or muscle weakness (43). As stated earlier, GSNOR$^{-/-}$ TA and lumbrical muscles showed no evidence of gross neuromuscular dysfunction or force deficits in spite of potential peripheral nerve dysfunction. Importantly, our data provide a compelling argument against myopathy or skeletal muscle weakness resulting from the absence of GSNOR. Therefore, it is likely that decreased grip strength in GSNOR$^{-/-}$ mice resulted from other causes such as reduced body size, lowered pain threshold, defective motor coordination, and/or lack of will to grip.

In addition, we found no atrophy in 6 month-old GSNOR$^{-/-}$ mice in contrast to a previous study (43). GSNOR$^{-/-}$ mice were smaller in absolute terms, with shorter nose-to-tail lengths and reduced muscle masses. However, when GSNOR$^{-/-}$ muscle masses were normalized to reduced body size, they were similar to wild-type controls. In addition, muscle cell areas and feret diameters, and MuRF1 and Atrogin 1 expression were normal in GSNOR$^{-/-}$ muscle, which, in addition to enhanced contractility, provide very strong evidence against atrophy. The reasons for this discrepancy are unclear but could relate to differences in iNOS expression between our study (where it was largely undetectable) and that of Montagna *et al.*, where iNOS was expressed at relatively high levels in both controls and GSNOR$^{-/-}$ muscle (43). An additional difference is that we measured muscle cell size in a fiber-specific way to avoid biasing our measurements. Nonetheless, our data argue against skeletal muscle atrophy in GSNOR$^{-/-}$ mice.

Our data also suggest potential insights into the nature of peripheral nerve dysfunction in GSNOR$^{-/-}$ mice. Peripheral nerve dysfunction may result from impaired sensory and/or motor neuron function. Montagna *et al.* showed that GSNOR$^{-/-}$ mice exhibit signs of sensory neuron dysfunction, including lowered pain thresholds to mechanical and thermal stimuli. Consistent with our findings, sensory neuron dysfunction would not necessarily impact muscle size, growth, or drive atrophy. In anesthetized mice, we find that GSNOR$^{-/-}$ TA muscles stimulated through the peroneal nerve are stronger and more fatigue resistant. These data are consistent with normal motor neuron function, because motor neuron defects typically cause muscle weakness or paralysis. Taken together, these data suggest that GSNOR deficiency may preferentially impair peripheral sensory neuron function.

Another interesting insight into the physiological roles of GSNO in skeletal muscle came from evidence that GSNOR inhibition impacted cGMP synthesis by sGC. These studies were performed as a control to provide evidence that the effects of GSNOR inhibition were independent of cGMP signaling. Baseline sGC activity was reduced by 45% in GSNOR$^{-/-}$ muscles, suggesting that GSNOR is required for normal cGMP synthesis in resting skeletal muscle. However, sGC-mediated cGMP synthesis was 50%, 90%, and 50% more responsive to the NO donor DETANO, sGC stimulator BAY 41, and sGC activator BAY 58 in GSNOR$^{-/-}$ muscles, respectively. These findings agree with recent reports that cGMP-dependent NO signaling may be modulated by S-nitrosylation (53, 54). However, in contrast to the present study, prolonged exposure to exogenous S-nitrosothiols desensitized sGC in smooth muscle cells (53). These data linking GSNOR and sGC activity, key players in ''cGMP-independent'' and ''cGMP-dependent'' signaling, suggest potential cross-talk or a close and necessary coordination between these two important NO effector pathways. Therefore, we cannot completely rule out a contribution of altered sGC-cGMP signaling to some of the phenotypic characteristics of GSNOR$^{-/-}$ mice.

In summary, we have used GSNOR$^{-/-}$ mice as a powerful experimental platform to advance our understanding of the physiological roles of GSNOR and denitrosylation in skeletal muscle. We provide compelling evidence that inhibition of GSNOR-mediated denitrosylation augments TA muscle contractility under physiological conditions, perhaps through an RyR1 hypernitrosylation-based mechanism. Our data also suggest new roles for GSNOR in type IIA fiber specification. Our findings argue against the proposition that GSNOR inhibition or RyR1 hypernitrosylation alone promotes myopathy and strengthen current evidence for the divergent roles of RyR1 S-nitrosylation under normal and disease conditions. Together, these data strengthen the argument that NO, specifically, and denitrosylation/nitrosylation balance, more generally, are important redox regulators of skeletal muscle contractile performance under physiological conditions.

Materials and Methods

S-nitrosoglutathione reductase knockout mice

Mice in a congenic C57Bl/6J background carrying targeted deletion of the coenzyme-binding domain of GSNOR, which eliminates GSNOR activity, have been previously described (41). Six-month-old male $GSNOR^{-/-}$ mice were used, unless otherwise stated. Age, gender, and strain-matched wild-type mice were used as controls. All experimental procedures performed on mice were approved by the Institutional Animal Care and Use Committees of the University of Miami.

Gene expression analysis by quantitative real-time PCR

Total RNA was isolated from frozen murine skeletal muscle using TRIzol reagent (Invitrogen) following the manufacturer's instructions. cDNAs were produced from 1 μg of total RNA using the iScript™ cDNA Synthesis Kit (Bio-Rad). Real-time PCR was performed using Sso Advanced Universal SYBR Green Supermix (Bio-Rad) on CFX Connect Real-Time PCR detection system (Bio-Rad) and Bio-Rad CFX Manager 3.1 software according to the manufacturer's instructions. Gene expression data were normalized to the Rps18 housekeeping gene and analyzed using the $\Delta\Delta C_T$ method (42). All primers and their sequences are listed in Supplementary Table S2. Primer efficiency was determined by a standard curve of cDNA samples in accordance with MIQE guidelines (12) and listed in Supplementary Table S3.

Determination of mtDNA levels by quantitative real-time PCR

Total DNA was isolated from TA muscle homogenates using the NucleoSpin Tissue XS kit (Clontech) according to the manufacturer's instructions. Amplification of nuclear and mtDNA was performed in a CFX96 real-time PCR system (Biorad) using specific primers for nucleus-encoded β-actin (ACTB) and mitochondrially encoded NADH Dehydrogenase 1 (ND1) genes, respectively. The amplification reaction was carried out using 5 ng of DNA in a 20 μl reaction mixture containing Sso Advance SYBR Green (Biorad) and primers by following the manufacturer's instructions. The levels of nuclear and mtDNA were calculated using the $\Delta\Delta$Ct method, then normalized to wild-type controls, and expressed as the ratio of ND1/ACTB (mtDNA/nDNA). Primers for ND1-forward: 5′CAGCCTGACCCATAGCCATA3′; ND1-reverse: 5′ ATTCTCCTTCTGTCAGGTCGAA3′; ACTB exon 6-forward: 5′ GCGAAGTACTCTGTGTGGA3′; ACTB exon 6-reverse: 5′CATCGTACTCCTGCTTGCTG3′.

Western immunoblotting

Freshly frozen muscle tissues were lysed in buffer containing 2% sodium dodecyl sulfate, 50 m*M* Tris-HCl (pH 6.8), and protease and phosphatase inhibitor cocktail tablets (Roche). Lysate protein content was quantified by BCA Protein Assay (Thermo Scientific). Thirty micrograms of protein was electrophoresed on 4–20% Mini-PROTEAN TGX Stain-Free Precast Gels (Bio-Rad) to determine loaded proteins on gels and to normalize immunoblotting signals by total visualized proteins. Stain-Free gels contained trihalo compounds that reacted with tryptophan residues after ultraviolet (UV) exposure to produce fluorescence, and then the loaded proteins were easily visualized by Bio-Rad ChemiDoc MP imager. Proteins after gel activation under UV for 2.5 min were then transferred to polyvinylidene fluoride membrane (Millipore). Transferred total protein on membranes was used for normalization using Bio-Rad ImageLab 5.2.1 software (Supplementary Fig. S1). Membranes were blocked with 5% (w/v) skim milk in Tris-buffered saline with Tween 20 (25 m*M* Tris, pH 7.4, 140 m*M* NaCl, 3 m*M* KCl, and 0.1% (v/v) Tween 20) for 1 h at room temperature and then incubated with primary antibodies overnight at 4°C. Primary antibodies used were as follows: rabbit anti-GSNOR (Proteintech), mouse anti-RyR (Thermo Fisher Scientific), rabbit anti-VDAC1, rabbit anti-phospho $nNOS^{1412}$, rabbit pan anti-nNOS, rabbit anti-α1 subunit of guanylate cyclase 1, and rabbit anti-β1 subunit of guanylate cyclase 1 (Sigma Aldrich). Note that ser^{1412} of nNOSα corresponds to ser^{1446} of nNOSμ due to the 34-amino-acid μ insert. MitoProfile® total OXPHOS antibody cocktail (Abcam) was used, which contains antibodies against NDUFB8 (Complex I or CI), SDHB (CII), UQCRC2 (CIII), MTCO1 (CIV), and ATP5A (CV). After incubation with donkey horseradish peroxidase-conjugated secondary antibodies (Jackson ImmunoResearch Laboratories), chemiluminescence from bands was visualized with SuperSignal West Femto substrate (Thermo Fisher) on a Chemidoc MP imaging system (Biorad).

Histopathological and central nucleation analyses

Freshly isolated hindlimb muscles from adult mice were placed in OCT embedding compound and flash frozen liquid nitrogen cooled 2-methylbutane. Ten micron-thick cryosections were cut from muscle midbellies; they were then stained with hematoxylin and eosin using standard methods. Muscles were inspected for signs of muscle disease, including: central nucleation, fiber size heterogeneity, and immune cell infiltration as described (29, 49, 50). The fraction of muscle cells with centrally localized nuclei (a marker of a muscle cell that has undergone a degeneration and regeneration event) was quantitated as previously described (50).

Determination of skeletal muscle fiber composition, fiber type area, and capillary density

To assess shifts in skeletal muscle fiber composition, 10-μm-thick cryosections from the muscle midbelly were fixed, blocked, and immunolabeled with a cocktail of monoclonal antibodies against type I (BA-D5), type IIA (SC-71), and type IIB (BF-F3) myosin heavy chains (Developmental Studies Hybridoma Bank) as described (49). Anti-myosin antibodies were detected using isotype-specific secondary antibodies: Alexa Fluor 350–labeled donkey anti-mouse IgG2B (BA-D5), Alexa Fluor 594–labeled donkey anti-mouse IgG1 (SC-71), and Alexa Fluor 488 donkey anti-mouse IgM (BF-F3). The incidence (number of positive muscle cells divided by the total number of muscle cells in the entire section) of type I, type IIA, and type IIB myosin heavy chain-positive muscle cells was determined manually. Unlabeled fibers were designated type IIX. Feret diameters and cross-sectional areas of 300 type IIX myofibers, 400 type IIB, and 100 type IIA myofibers were determined per mouse from spatially calibrated images using Image J 1.46r software (55). Feret's diameter is the longest distance between any two points along the myofiber selection

boundary and is a reliable measure of muscle cell size, because it is less susceptible to sectioning angle than cross-sectional area (10). To determine capillary blood vessel density, muscle sections were immunolabeled with rabbit anti-CD31 polyclonal antibody (Abcam) and the total number of CD31 (an endothelial cell marker)-positive capillaries in each cryosection were counted manually. Capillary densities were expressed as the number of CD31-positive capillaries per mm^2.

Automated bright-field and immunofluorescence microscopy

Automated capture of images covering the entire area of a muscle cross-section was performed at 20× magnification using a DP80 digital camera (Olympus), and CellSens software operated an automated tiling system comprising an Olympus BX50 upright microscope fitted with a Prior Scientific motorized *x–y* stage. Composite images of whole muscle sections labeled with hematoxylin and eosin were formed by stitching individual color images that were captured sequentially together into a single composite image. For fluorescent images, individual images of Alexa 350, 488, and 594 fluorescence emissions (as appropriate) were captured sequentially; they were then automatically stitched together to form a composite image of the entire muscle cross-section.

sGC activity measurements

sGC enzyme activity was measured as previously described (13). Briefly, gastrocnemius skeletal muscles were harvested and homogenized in buffer containing 50 m*M* Tris.HCl (pH 7.6), 1 m*M* EDTA, 1 m*M* dithiothreitol, and 2 mM phenylmethylsulfonyl fluoride. Extracts were centrifuged at 20,000 *g* for 20 min at 4°C. Supernatants containing 50 μg protein were incubated for 10 min at 37°C with 50 m*M* Tris.HCl (pH 7.5), 4 m*M* $MgCl_2$, 0.5 m*M* 1-methyl-3-isobutylxanthine, 7.5 m*M* creatine phosphate, 0.2 mg/ml creatine phosphokinase, 1 m*M* L-NAME, and 1 m*M* GTP with or without 10 μ*M* of NO donor DETA-NO, 100 μ*M* sGC activator BAY 58-2667 (cinaciguat), or 1 m*M* of sGC stimulator BAY 41-2272. The reaction was terminated with 0.05 *M* HCl. cGMP was measured by immunoassay (Cayman Chemical). sGC activity was expressed as picomoles of cGMP synthesized per minute per milligram of gastrocnemius muscle protein per minute.

In situ *measurement of TA strength and fatigue resistance*

Tests of skeletal muscle strength and fatigue resistance were performed on the TA muscle *in vivo* in anesthetized adult mice as described with minor modifications (48). Blood delivery and innervation to the muscle are maintained, providing ''gold standard'' physiological conditions for the measurement of fatigue resistance (2). Mice were anesthetized with intraperitoneal injections of Avertin and positioned on a 37°C heated platform. The distal tendon of the TA muscle was attached to the lever arm of a 305C-LR servomotor (Aurora Scientific Instruments), and contractions were elicited by electrical bipolar stimulation of the peroneal nerve. The Dynamic Muscle Control and Analysis Software Suite (Aurora Scientific Instruments) was used for data collection and analysis. The partially exposed muscle surface was kept moist for the duration of the experiment by application of prewarmed isotonic saline. The muscle was adjusted to an optimum length (L_o) that produced the maximum isometric tetanic force (P_o). To investigate the force–frequency relationship and potential dependence of force output on stimulation frequency, TA muscles at L_o were tetanically stimulated over a range of submaximal to maximal tetanic stimulation frequencies (10–200 Hz), with 1 min intervals between stimulations to avoid fatigue. Force outputs over the 5–200 Hz range were normalized to the maximal tetanic force (P_o) generation, which was typically achieved at 200 Hz. P_o was normalized to the cross-sectional area of the muscle to generate a specific force (sP_o)–frequency curve. At the completion of testing, the greatest specific force (sP_o) value was used as a measure of the intrinsic strength of the TA muscle. Isometric tetanic force and fiber composition studies, the twitch properties of TA muscles were also investigated. Maximum twitch force, specific twitch force, time to peak twitch force, and time for twitch force to return to half the maximum value were determined. To measure skeletal muscle fatigue resistance, TA muscles were subjected to 4 min of repeated maximal tetanic contractions as previously described. Muscles were maximally stimulated (40 V, 200 Hz, 300 ms) every 2 s for 4 min. Force output was normalized to the force produced by the first and strongest contraction. To ensure fatigue-associated force loss was reversible and not due to muscle damage, force recovery was assessed at 1, 3, and 5 min after the completion of the fatigue protocol.

Measurement of intracellular Ca^{2+} and force in lumbrical skeletal muscles in vitro

The murine lumbrical muscle model system was used to simultaneously measure fluxes in force and intracellular Ca^{2+} as described with minor changes (66). Lumbrical muscles were dissected from hindpaws into a Krebs–Henseleit solution containing 30 m*M* 2,3-butanedione monoxime that was saturated with 95% O_2–5% CO_2. Intact lumbrical muscles were then mounted in the Guth muscle research system (Scientific Instruments) that can simultaneously measures changes in myofiber force output and fluorescent emissions from Ca^{2+}-sensitive fluorescent indicators (66). For force measurements, the distal lumbrical muscle tendon was attached to a servomotor, whereas the proximal end was attached to the force transducer. Mounted lumbrical muscles were adjusted to optimal length (Lo), where maximum twitch force output was obtained. The muscle was stimulated at 100 Hz, and changes in tetanic force output were recorded. The values reported represent the mean force value of 100 successive stimulations. Specific force was calculated by dividing the maximum tetanic force by lumbrical muscle cross-sectional area. For intracellular Ca^{2+} transient measurements, lumbrical muscles were loaded with high-affinity 5 μ*M* fura 2-AM Ca^{2+} indicator (Invitrogen) in oxygenated Krebs–Henseleit solution containing 0.5% cremophore to increase fura solubility for 1 h. Fluorescent emissions from the 340 nm and 380 nm excitation of fura-2-AM were sampled by a signal sorter and recorded. The time resolution of the 340/380 fluorescence ratio measurements was 4 ms. Background fluorescence from 340 and 380 nm excitation of unloaded lumbrical preparations was subtracted before the fluorescence 340/380 was calculated and plotted along with force. Corrected 340/380 ratios were used to calculate relative changes in intracellular Ca^{2+}. The values reported

represent the mean intracellular Ca^{2+} value of the 100 successive stimulations. All measurements were made at room temperature (21°C). To investigate potential effects of the frequency of stimulation on force output and intracellular Ca^{2+} levels, force–frequency and Ca^{2+}–frequency relationships were investigated. Lumbrical muscles at L_o were tetanically stimulated over a range of stimulation frequencies (5–100 Hz), with at least 8 s between stimulations to avoid fatigue. Force outputs and Ca^{2+} levels were determined and normalized to the maximal tetanic force (P_o) generation, which was typically achieved at 100 Hz. To mimic fatiguing conditions, lumbrical muscles were subjected to a series of 100 maximal tetanic stimulations, with progressively shorter intervals (ranging from 0.5 to 8 s) between successive stimulations. The more strenuous fatiguing conditions occurred with a 0.5 s interval between successive stimulations, whereas single maximal tetanic stimulations every 8 s did not cause muscle fatigue.

S-nitrosylation analysis by S-nitrosothiol resin-assisted capture

RyR1 S-nitrosylation analysis by S-nitrosothiol resin-assisted capture (SNO-RAC) assay was performed as described due to its increased efficiency in detecting high-molecular-weight S-nitrosylated proteins (25). All chemicals were purchased from Sigma Aldrich, unless otherwise noted. Experiments were conducted in a dark room or with opaque brown tubes where appropriate. Skeletal muscle was homogenized in 2% sodium dodecyl sulfate, 50 m*M* Tris-HCl (pH 6.8) with protease and phosphatase inhibitor cocktails (Roche Applied Science) and then briefly sonicated. Free cysteines were blocked with *S*-methylmethane-thiosulfonate in the presence of sodium dodecyl sulfate for 20 min. Then, the protein lysate was incubated with 100% acetone at −20°C for 20 min and centrifuged at 15,000 *g* for 20 min. The pellet was washed with 70% acetone and resuspended in HENS buffer (250 m*M* Hepes, 1 m*M* EDTA, 0.1 m*M* neocuproine pH 7.7). Ten microliters of input samples was taken from each tube. Thiol-reactive resin was activated by incubating with water for 30 min. Sodium ascorbate was added to reduce the SNOs to thiols (20 m*M* final concentration). Omission of ascorbate served as a negative control. Newly formed thiols of the protein lysate were captured by incubation with thiol-reactive resin for 3–5 h in the dark. After incubation, the resin-protein complex was washed five times with HEN buffer. Resin-captured proteins were eluted with 50 μl elution buffer (20 m*M* HEPES, 100 m*M* NaCl, 1 m*M* EDTA, 100 m*M* β-mercaptoethanol) at room temperature with frequent agitation and then heated at 95°C for 5 min in nonreducing SDS–PAGE loading buffer.

Analysis of mitochondria respiratory complex I, III, and IV activities

Frozen TA muscle tissue was resuspended in PBS containing a protease inhibitor cocktail (Roche) and homogenized (15–20 strokes) using a hand-held motorized homogenizer. Samples were centrifuged at 1000 rpm for 5 min to remove tissue remnants, and the supernatant was used to determine enzymatic activity of mitochondrial respiratory chain complexes I, III, and IV. Respiratory complex activity was determined spectrophotometrically with a Synergy H1 plate reader (BioTek) using the kinetics mode of Gen5 software (BioTek). Complex I activity was determined by following NADH oxidation at 340 nm in a 200 μl reaction mixture containing 20 m*M* KPO_4 pH 8.0, 200 μ*M* NADH, 300 μ*M* KCN, 0.1 mg/ml BSA, and 100 μ*M* CoenzymeQ1 with or without 10 μ*M* rotenone to determine reaction specificity. Complex III activity was measured by following cytochrome c reduction at 550 nm in a 200 μl reaction mixture containing 50 m*M* KPO_4 buffer pH7.5, 3 m*M* KCN, 1 m*M* EDTA, 50 μ*M* cytochrome c, 0.05% lauryl maltoside, and 10 μ*M* CoQ2-H2 in the presence or absence of 10 μg/ml antimycin A to determine reaction specificity. Complex IV activity was determined by following the oxidation of reduced cytochrome c at 550 nm in a 200 μl reaction mixture containing 10 m*M* KPO_4 pH 6.8, 40 μ*M* reduced cytochrome c, and 2.4 m*M* lauryl maltoside. The reaction was terminated with 300 μ*M* KCN. Enzymatic activities are represented in mmol/min/mg of protein or as respiratory complex activity normalized to citrate synthase.

Citrate synthase activity measurement

Citrate synthase activity was measured by determining the change in absorbance of DTNB at 412 nm in a 200 μl reaction mixture containing 50 m*M* Tris-HCl pH 7.5, 200 μ*M* acetyl CoA, 0.2% Triton-X100, 100 μ*M* dithio-bis-nitrobenzoic acid, and 1 m*M* oxaloacetate.

Statistical analyses

All values are reported as mean ± standard error of the mean. Protein and mRNA expression data were normalized by dividing all values by the mean of the wild-type control group. Significant differences between two group means were discerned by unpaired *t*-tests for normally distributed variables. Normality was determined using the D'Agostino–Pearson test where appropriate. Two-way ANOVA followed by Tukey's multiple-comparison *post hoc* tests between paired groups were used for analyses of muscle fatigue and force–/Ca^{2+}–frequency relationships. Statistical calculations were performed using Prism v 6.07 (Graphpad Software, Inc.); p values of <0.05 were considered significant.

Acknowledgments

The authors would like to thank Dr. Kimberley Craven for editing services. JP was funded by NIH grant 1R03AR066805-01 and the Department of Defense grant MD140021. JMH was funded by NIH grants R01HL110737, R01HL107110, R01HL084275, and 5UM1HL113460 and grants from the Starr Foundation and the Soffer Family Foundation. YC was funded by a predoctoral fellowship from the American Heart Association. The content is solely the responsibility of the authors and does not necessarily represent the official views of the NIH or DOD.

Author Disclosure Statement

Dr. Hare reported having a patent for cardiac cell-based therapy. He holds equity in Vestion and maintains a professional relationship with Vestion as a consultant and member of the Board of Directors and the Scientific Advisory Board. Vestion Inc. did not play a role in the design and conduct of this study. The other authors report no conflicts.

References

1. Adamo CM, Dai DF, Percival JM, Minami E, Willis MS, Patrucco E, Froehner SC, and Beavo JA. Sildenafil reverses cardiac dysfunction in the mdx mouse model of Duchenne muscular dystrophy. *Proc Natl Acad Sci U S A* 107: 19079–19083, 2010.
2. Allen DG, Lamb GD, and Westerblad H. Skeletal muscle fatigue: cellular mechanisms. *Physiol Rev* 88: 287–332, 2008.
3. Andersson DC, Betzenhauser MJ, Reiken S, Meli AC, Umanskaya A, Xie W, Shiomi T, Zalk R, Lacampagne A, and Marks AR. Ryanodine receptor oxidation causes intracellular calcium leak and muscle weakness in aging. *Cell Metab* 14: 196–207, 2011.
4. Andersson DC, Meli AC, Reiken S, Betzenhauser MJ, Umanskaya A, Shiomi T, D'Armiento J, and Marks AR. Leaky ryanodine receptors in beta-sarcoglycan deficient mice: a potential common defect in muscular dystrophy. *Skelet Muscle* 2: 9, 2012.
5. Aracena P, Sanchez G, Donoso P, Hamilton SL, and Hidalgo C. S-glutathionylation decreases Mg2+ inhibition and S-nitrosylation enhances Ca2+ activation of RyR1 channels. *J Biol Chem* 278: 42927–42935, 2003.
6. Baum O, Vieregge M, Koch P, Gul S, Hahn S, Huber-Abel FA, Pries AR, and Hoppeler H. Phenotype of capillaries in skeletal muscle of nNOS-knockout mice. *Am J Physiol Regul Integr Comp Physiol* 304: R1175–R1182, 2013.

6a. Beigi F, Gonzalez DR, Minhas KM, Sun QA, Foster MW, Khan SA, Treuer AV, Dulce RA, Harrison RW, Saraiva RM, Premer C, Schulman IH, Stamler JS, and Hare JM. Dynamic denitrosylation via S-nitrosoglutathione reductase regulates cardiovascular function. *Proc Natl Acad Sci U S A*. 109: 4314–4319, 2012.

7. Bellinger AM, Reiken S, Carlson C, Mongillo M, Liu X, Rothman L, Matecki S, Lacampagne A, and Marks AR. Hypernitrosylated ryanodine receptor calcium release channels are leaky in dystrophic muscle. *Nat Med* 15: 325–330, 2009.
8. Bellinger AM, Reiken S, Dura M, Murphy PW, Deng SX, Landry DW, Nieman D, Lehnart SE, Samaru M, LaCampagne A, and Marks AR. Remodeling of ryanodine receptor complex causes ''leaky'' channels: a molecular mechanism for decreased exercise capacity. *Proc Natl Acad Sci U S A* 105: 2198–2202, 2008.
9. Bodine SC and Baehr LM. Skeletal muscle atrophy and the E3 ubiquitin ligases MuRF1 and MAFbx/atrogin-1. *Am J Physiol Endocrinol Metab* 307: E469–E484, 2014.
10. Briguet A, Courdier-Fruh I, Foster M, Meier T, and Magyar JP. Histological parameters for the quantitative assessment of muscular dystrophy in the mdx-mouse. *Neuromuscul Disord* 14: 675–682, 2004.
11. Brown GC and Cooper CE. Nanomolar concentrations of nitric oxide reversibly inhibit synaptosomal respiration by competing with oxygen at cytochrome oxidase. *FEBS Lett* 356: 295–298, 1994.
12. Bustin SA, Benes V, Garson JA, Hellemans J, Huggett J, Kubista M, Mueller R, Nolan T, Pfaffl MW, Shipley GL, Vandesompele J, and Wittwer CT. The MIQE guidelines: minimum information for publication of quantitative real-time PCR experiments. *Clin Chem* 55: 611–622, 2009.
13. Buys ES, Sips P, Vermeersch P, Raher MJ, Rogge E, Ichinose F, Dewerchin M, Bloch KD, Janssens S, and Brouckaert P. Gender-specific hypertension and responsiveness to nitric oxide in sGCalpha1 knockout mice. *Cardiovasc Res* 79: 179–186, 2008.
14. Cao Y, Gomes SA, Rangel EB, Paulino EC, Fonseca TL, Li J, Teixeira MB, Gouveia CH, Bianco AC, Kapiloff MS, Balkan W, and Hare JM. S-nitrosoglutathione reductase-dependent PPARgamma denitrosylation participates in MSC-derived adipogenesis and osteogenesis. *J Clin Invest* 125: 1679–1691, 2015.
15. Church JE, Gehrig SM, Chee A, Naim T, Trieu J, McConell GK, and Lynch GS. Early functional muscle regeneration after myotoxic injury in mice is unaffected by nNOS absence. *Am J Physiol Regul Integr Comp Physiol* 301: R1358–R1366, 2011.
16. Cleeter MW, Cooper JM, Darley-Usmar VM, Moncada S, and Schapira AH. Reversible inhibition of cytochrome c oxidase, the terminal enzyme of the mitochondrial respiratory chain, by nitric oxide. Implications for neurodegenerative diseases. *FEBS Lett* 345: 50–54, 1994.
17. Clementi E, Brown GC, Feelisch M, and Moncada S. Persistent inhibition of cell respiration by nitric oxide: crucial role of S-nitrosylation of mitochondrial complex I and protective action of glutathione. *Proc Natl Acad Sci U S A* 95: 7631–7636, 1998.
18. Conley KE, Jubrias SA, Amara CE, and Marcinek DJ. Mitochondrial dysfunction: impact on exercise performance and cellular aging. *Exerc Sport Sci Rev* 35: 43–49, 2007.
19. De Palma C, Morisi F, Pambianco S, Assi E, Touvier T, Russo S, Perrotta C, Romanello V, Carnio S, Cappello V, Pellegrino P, Moscheni C, Bassi MT, Sandri M, Cervia D, and Clementi E. Deficient nitric oxide signalling impairs skeletal muscle growth and performance: involvement of mitochondrial dysregulation. *Skelet Muscle* 4: 22, 2014.
20. Derbyshire ER and Marletta MA. Structure and regulation of soluble guanylate cyclase. *Annu Rev Biochem* 81: 533–559, 2012.
21. Durham WJ, Aracena-Parks P, Long C, Rossi AE, Goonasekera SA, Boncompagni S, Galvan DL, Gilman CP, Baker MR, Shirokova N, Protasi F, Dirksen R, and Hamilton SL. RyR1 S-nitrosylation underlies environmental heat stroke and sudden death in Y522S RyR1 knockin mice. *Cell* 133: 53–65, 2008.
22. Dutka TL, Mollica JP, Posterino GS, and Lamb GD. Modulation of contractile apparatus Ca2+ sensitivity and disruption of excitation-contraction coupling by S-nitrosoglutathione in rat muscle fibres. *J Physiol* 589: 2181–2196, 2011.
23. Eu JP, Hare JM, Hess DT, Skaf M, Sun J, Cardenas-Navina I, Sun QA, Dewhirst M, Meissner G, and Stamler JS. Concerted regulation of skeletal muscle contractility by oxygen tension and endogenous nitric oxide. *Proc Natl Acad Sci U S A* 100: 15229–15234, 2003.
24. Eu JP, Sun J, Xu L, Stamler JS, and Meissner G. The skeletal muscle calcium release channel: coupled O2 sensor and NO signaling functions. *Cell* 102: 499–509, 2000.
25. Forrester MT, Thompson JW, Foster MW, Nogueira L, Moseley MA, and Stamler JS. Proteomic analysis of S-nitrosylation and denitrosylation by resin-assisted capture. *Nat Biotechnol* 27: 557–559, 2009.
26. Foster MW, Hess DT, and Stamler JS. Protein S-nitrosylation in health and disease: a current perspective. *Trends Mol Med* 15: 391–404, 2009.
27. Foster MW and Stamler JS. New insights into protein S-nitrosylation. Mitochondria as a model system. *J Biol Chem* 279: 25891–25897, 2004.
28. Friebe A and Koesling D. The function of NO-sensitive guanylyl cyclase: what we can learn from genetic mouse models. *Nitric Oxide* 21: 149–156, 2009.

29. Froehner SC, Reed SM, Anderson KN, Huang PL, and Percival JM. Loss of nNOS inhibits compensatory muscle hypertrophy and exacerbates inflammation and eccentric contraction-induced damage in mdx mice. *Hum Mol Genet* 24: 492–505, 2015.
30. Galkin A and Moncada S. S-nitrosation of mitochondrial complex I depends on its structural conformation. *J Biol Chem* 282: 37448–37453, 2007.
31. Gentil C, Leturcq F, Ben Yaou R, Kaplan JC, Laforet P, Penisson-Besnier I, Espil-Taris C, Voit T, Garcia L, and Pietri-Rouxel F. Variable phenotype of del45-55 Becker patients correlated with nNOSmu mislocalization and RYR1 hypernitrosylation. *Hum Mol Genet* 21: 3449–3460, 2012.
32. Gould N, Doulias PT, Tenopoulou M, Raju K, and Ischiropoulos H. Regulation of protein function and signaling by reversible cysteine S-nitrosylation. *J Biol Chem* 288: 26473–26479, 2013.
33. Haldar SM and Stamler JS. S-nitrosylation: integrator of cardiovascular performance and oxygen delivery. *J Clin Invest* 123: 101–110, 2013.
34. Hess DT and Stamler JS. Regulation by S-nitrosylation of protein post-translational modification. *J Biol Chem* 287: 4411–4418, 2012.
35. Hinchee-Rodriguez K, Garg N, Venkatakrishnan P, Roman MG, Adamo ML, Masters BS, and Roman LJ. Neuronal nitric oxide synthase is phosphorylated in response to insulin stimulation in skeletal muscle. *Biochem Biophys Res Commun* 435: 501–505, 2013.
36. Hong YH, Frugier T, Zhang X, Murphy RM, Lynch GS, Betik AC, Rattigan S, and McConell GK. Glucose uptake during contraction in isolated skeletal muscles from neuronal nitric oxide synthase mu knockout mice. *J Appl Physiol (1985)* 118: 1113–1121, 2015.
37. Iglesias DE, Bombicino SS, Valdez LB, and Boveris A. Nitric oxide interacts with mitochondrial complex III producing antimycin-like effects. *Free Radic Biol Med* 89: 602–613, 2015.
38. Kobzik L, Reid MB, Bredt DS, and Stamler JS. Nitric oxide in skeletal muscle. *Nature* 372: 546–548, 1994.
39. Li D, Yue Y, Lai Y, Hakim CH, and Duan D. Nitrosative stress elicited by nNOSmicro delocalization inhibits muscle force in dystrophin-null mice. *J Pathol* 223: 88–98, 2011.
40. Lima B, Lam GK, Xie L, Diesen DL, Villamizar N, Nienaber J, Messina E, Bowles D, Kontos CD, Hare JM, Stamler JS, and Rockman HA. Endogenous S-nitrosothiols protect against myocardial injury. *Proc Natl Acad Sci U S A* 106: 6297–6302, 2009.
41. Liu L, Yan Y, Zeng M, Zhang J, Hanes MA, Ahearn G, McMahon TJ, Dickfeld T, Marshall HE, Que LG, and Stamler JS. Essential roles of S-nitrosothiols in vascular homeostasis and endotoxic shock. *Cell* 116: 617–628, 2004.
42. Livak KJ and Schmittgen TD. Analysis of relative gene expression data using real-time quantitative PCR and the 2(-Delta Delta C(T)) Method. *Methods* 25: 402–408, 2001.
43. Montagna C, Di Giacomo G, Rizza S, Cardaci S, Ferraro E, Grumati P, De Zio D, Maiani E, Muscoli C, Lauro F, Ilari S, Bernardini S, Cannata S, Gargioli C, Ciriolo MR, Cecconi F, Bonaldo P, and Filomeni G. S-nitrosoglutathione reductase deficiency-induced S-nitrosylation results in neuromuscular dysfunction. *Antioxid Redox Signal* 21: 570–587, 2014.
44. Nisoli E, Clementi E, Paolucci C, Cozzi V, Tonello C, Sciorati C, Bracale R, Valerio A, Francolini M, Moncada S, and Carruba MO. Mitochondrial biogenesis in mammals: the role of endogenous nitric oxide. *Science* 299: 896–899, 2003.
45. Nisoli E, Falcone S, Tonello C, Cozzi V, Palomba L, Fiorani M, Pisconti A, Brunelli S, Cardile A, Francolini M, Cantoni O, Carruba MO, Moncada S, and Clementi E. Mitochondrial biogenesis by NO yields functionally active mitochondria in mammals. *Proc Natl Acad Sci U S A* 101: 16507–16512, 2004.
46. Percival JM. nNOS regulation of skeletal muscle fatigue and exercise performance. *Biophys Rev* 3: 209–217, 2011.
47. Percival JM, Adamo CM, Beavo JA, and Froehner SC. Evaluation of the therapeutic utility of phosphodiesterase 5A inhibition in the mdx mouse model of duchenne muscular dystrophy. *Handb Exp Pharmacol* 204: 323–344, 2011.
48. Percival JM, Anderson KN, Gregorevic P, Chamberlain JS, and Froehner SC. Functional deficits in nNOSmu-deficient skeletal muscle: myopathy in nNOS knockout mice. *PLoS One* 3: e3387, 2008.
49. Percival JM, Anderson KN, Huang P, Adams ME, and Froehner SC. Golgi and sarcolemmal neuronal NOS differentially regulate contraction-induced fatigue and vasoconstriction in exercising mouse skeletal muscle. *J Clin Invest* 120: 816–826, 2010.
50. Percival JM, Whitehead NP, Adams ME, Adamo CM, Beavo JA, and Froehner SC. Sildenafil reduces respiratory muscle weakness and fibrosis in the mdx mouse model of Duchenne muscular dystrophy. *J Pathol* 228: 77–87, 2012.
51. Piantadosi CA and Suliman HB. Redox regulation of mitochondrial biogenesis. *Free Radic Biol Med* 53: 2043–2053, 2012.
52. Rameau GA, Tukey DS, Garcin-Hosfield ED, Titcombe RF, Misra C, Khatri L, Getzoff ED, and Ziff EB. Biphasic coupling of neuronal nitric oxide synthase phosphorylation to the NMDA receptor regulates AMPA receptor trafficking and neuronal cell death. *J Neurosci* 27: 3445–3455, 2007.
53. Sayed N, Baskaran P, Ma X, van den Akker F, and Beuve A. Desensitization of soluble guanylyl cyclase, the NO receptor, by S-nitrosylation. *Proc Natl Acad Sci U S A* 104: 12312–12317, 2007.
54. Sayed N, Kim DD, Fioramonti X, Iwahashi T, Duran WN, and Beuve A. Nitroglycerin-induced S-nitrosylation and desensitization of soluble guanylyl cyclase contribute to nitrate tolerance. *Circ Res* 103: 606–614, 2008.
55. Schneider CA, Rasband WS, and Eliceiri KW. NIH Image to ImageJ: 25 years of image analysis. *Nat Methods* 9: 671–675, 2012.
56. Shankar RR, Wu Y, Shen HQ, Zhu JS, and Baron AD. Mice with gene disruption of both endothelial and neuronal nitric oxide synthase exhibit insulin resistance. *Diabetes* 49: 684–687, 2000.
57. Shiva S, Sack MN, Greer JJ, Duranski M, Ringwood LA, Burwell L, Wang X, MacArthur PH, Shoja A, Raghavachari N, Calvert JW, Brookes PS, Lefer DJ, and Gladwin MT. Nitrite augments tolerance to ischemia/reperfusion injury via the modulation of mitochondrial electron transfer. *J Exp Med* 204: 2089–2102, 2007.
58. Silvagno F, Xia H, and Bredt DS. Neuronal nitric-oxide synthase-mu, an alternatively spliced isoform expressed in differentiated skeletal muscle. *J Biol Chem* 271: 11204–11208, 1996.
59. Stoyanovsky D, Murphy T, Anno PR, Kim YM, and Salama G. Nitric oxide activates skeletal and cardiac ryanodine receptors. *Cell Calcium* 21: 19–29, 1997.
60. Sun J, Xin C, Eu JP, Stamler JS, and Meissner G. Cysteine-3635 is responsible for skeletal muscle ryanodine receptor

modulation by NO. *Proc Natl Acad Sci U S A* 98: 11158–11162, 2001.
61. Sun J, Xu L, Eu JP, Stamler JS, and Meissner G. Nitric oxide, NOC-12, and S-nitrosoglutathione modulate the skeletal muscle calcium release channel/ryanodine receptor by different mechanisms. An allosteric function for O2 in S-nitrosylation of the channel. *J Biol Chem* 278: 8184–8189, 2003.
62. Sun QA, Wang B, Miyagi M, Hess DT, and Stamler JS. Oxygen-coupled redox regulation of the skeletal muscle ryanodine receptor/Ca2+ release channel (RyR1): sites and nature of oxidative modification. *J Biol Chem* 288: 22961–22971, 2013.
63. Suzuki N, Motohashi N, Uezumi A, Fukada S, Yoshimura T, Itoyama Y, Aoki M, Miyagoe-Suzuki Y, and Takeda S. NO production results in suspension-induced muscle atrophy through dislocation of neuronal NOS. *J Clin Invest* 117: 2468–2476, 2007.
64. Thomas GD, Shaul PW, Yuhanna IS, Froehner SC, and Adams ME. Vasomodulation by skeletal muscle-derived nitric oxide requires alpha-syntrophin-mediated sarcolemmal localization of neuronal Nitric oxide synthase. *Circ Res* 92: 554–560, 2003.
65. Tsikas D. Potential problems and pitfalls with the use of S-nitrosoglutathione and other S-nitrosothiols in physiology-oriented basic science. *J Physiol* 590: 6247–6248, 2012.
66. Wang Y and Kerrick WG. The off rate of Ca(2+) from troponin C is regulated by force-generating cross bridges in skeletal muscle. *J Appl Physiol (1985)* 92: 2409–2418, 2002.
67. Yamada T, Fedotovskaya O, Cheng AJ, Cornachione AS, Minozzo FC, Aulin C, Friden C, Turesson C, Andersson DC, Glenmark B, Lundberg IE, Rassier DE, Westerblad H, and Lanner JT. Nitrosative modifications of the Ca^{2+} release complex and actin underlie arthritis-induced muscle weakness. *Ann Rheum Dis* 74: 1907–1914, 2015.

Address correspondence to:
Dr. Justin M. Percival
Department of Molecular and Cellular Pharmacology (R-189)
University of Miami Miller School of Medicine
PO Box 016189
Miami, FL 33101

E-mail: j.percival@med.miami.edu

Date of first submission to ARS Central, October 27, 2015; date of final revised submission, July 11, 2016; date of acceptance, July 12, 2016.

Abbreviations Used

ATP = adenosine triphosphate
ATP5a = mitochondrial ATP synthase alpha-subunit
BSA = bovine serum albumin
cGMP = cyclic guanosine monophosphate
CoQ2-H2 = coenzyme Q analog
DETA-NO = diethylenetriamine NONOate
Dia = diaphragm
DTNB = 5,5′-dithiobis-(2-nitrobenzoic acid)
Gas = gastrocnemius
GSNO = S-nitrosoglutathione
GSNOR = S-nitrosoglutathione reductase
GTP = guanosine-5′-triphosphate
HIF1α = hypoxia-inducible factor 1 alpha subunit
KCN = potassium cyanide
KPO_4 = potassium phosphate
L-NAME = L-N^G-Nitroarginine methyl ester
MTCO1 = mitochondrial Cytochrome C Oxidase I
NADH = reduced nicotinamide adenine dinucleotide
ND1 = mitochondrially encoded NADH dehydrogenase 1
NDUFB8 = NADH dehydrogenase 1 beta subcomplex, 8
nNOS = neuronal nitric oxide synthase
NO = nitric oxide
PGC1α = peroxisome proliferative activated receptor, gamma, coactivator 1, alpha
Quad = quadriceps
RyR = ryanodine receptor
SDHB = succinate dehydrogenase complex, subunit B
sGC = soluble guanylate cyclase
SNO-RAC = S-nitrosothiol resin-assisted capture
Sol = soleus
TA = tibialis anterior
UQCRC2 = ubiquinol-cytochrome c reductase core protein II
VDAC1 = voltage-dependent Anion Channel 1
VEGF = vascular endothelial growth factor
WT = wild type